Astron. Astrophys. 338, 413–434 (1998)

ASTRONOMY
AND
ASTROPHYSICS

Models of the long-term evolution of the Galactic disk with viscous flows and gas infall

R. Thon and H. Meusinger

Thüringer Landessternwarte Tautenburg, Sternwarte 5, D-07778 Tautenburg, Germany

Received 23 December 1997 / Accepted 22 July 1998

Abstract. Radial gas flows induced by viscosity may significantly redistribute the gas component in galactic disks. On the condition that the timescale of the viscous transport is comparable to the star formation timescale, this process naturally explains the observed exponential stellar density profiles in disks independent of the density profiles of the initial disks. We discuss models for the chemical and dynamical evolution of the Galactic disk which combine viscous radial gas flows with infall of external gas onto the disk, and infall-induced radial gas flows. The main goal of this study is the confrontation of model results with a large set of observational constraints from the Galactic disk. The star formation rate and the viscosity in the interstellar medium are parametrised as usual in modelling the evolution of a viscous star forming disk. The element abundance evolution for oxygen and iron is driven by supernovae of types Ia and II. Chemical inhomogeneities are taken into account for the interstellar medium at given time and Galactocentric distance.

In the result of a large number of model computations, we found several distinct models which provide an acceptable fit to most of the observational data. However, the models are not appropriate to fit all observed details, partly due to the simple description of the star formation rate. We discuss the evolution of radial abundance gradients. Although viscous models generally produce gradients, their values are typically only $-0.03\,\mathrm{dex\,kpc}^{-1}$ if we adopt the initial gas density distribution of an isothermal sphere. Several processes are discussed which can enhance the gradients.

Viscous evolution generates a strong mass concentration in the inner few kpc. We compare the properties of the central stellar population in the models with the Galactic bulge and discuss the possible relationship between viscous flows and bulge formation. Furthermore, we propose that the observed radial gas density distribution in the innermost disk may be produced by strongly enhanced viscosity in that region, e.g. due to a central bar.

Key words: hydrodynamics – Galaxy: center – Galaxy: evolution – Galaxy: solar neighbourhood

Send offprint requests to: H. Meusinger

1. Introduction

The secular evolution of disk galaxies may be significantly influenced by radial gas flows (e.g., Lacey & Fall 1985; Köppen 1994; Courthau et al. 1996). Especially, gas flows due to viscosity have become attractive to explain the observed radial profiles of disks. Although the physical nature of the viscosity is essentially unknown, several aspects of viscous galactic evolution have been studied in detail over the last decade (e.g., Lin & Pringle 1987; Clarke 1989; Sommer-Larsen & Yoshii 1989, 1990; Olivier et al. 1991; Fröhlich 1994; Firmani et al. 1996). It was established that fundamental properties of disks can be reproduced in the context of viscous evolution: The observed exponential stellar disk profiles can be explained as a natural consequence of the redistribution of angular momentum by a viscous gas drift. Moreover, viscous evolution generates a flat transition between the outer (halo-dominated) and the inner (disk-bulge-dominated) rotation curve of spiral galaxies (Saio & Yoshii 1990; Tsujimoto et al. 1995 a) and provides a natural explanation for this "conspiracy" between dark and luminous matter.

On the other hand, stringent observational constraints are not fit by viscous gas flow models but require additional assumptions like gas infall. It has been suggested long ago (Larson 1972; Lynden-Bell 1975; Pagel & Patchett 1975) that prolonged infall of chemically unenriched gas was an important aspect in Galactic evolution. More recent studies invoking gas infall to describe the chemical evolution of the local region in the Galactic disk include those by van den Hoek & de Jong (1997), Pilyugin & Edmunds (1996), Prantzos & Aubert (1995), and Meusinger (1994). If gas infall is important, the Galactic disk is not adequately described by a simple multi-zone model with separated zones (Mayor & Vigroux 1981): To maintain consistency, radial gas flows have to be taken into account as a dynamical consequence of infall. Such kind of models have been investigated in detail by Pitts & Tayler (1989) and Chamcham & Tayler (1994).

The modification of viscous models by the addition of infall seems to be a more realistic description of galactic evolution. In this paper we present hydrodynamic "hybrid" models for the chemical evolution of the Galactic disk which include the effects of viscosity, gas infall and infall-induced radial gas flows. Heavy element production from supernovae (SNe) of types Ia

and II is taken into account. The models are relatively simple compared to chemodynamical models involving a multiphase interstellar medium (Hensler et al. 1994; Samland et al. 1997). Nevertheless, it is useful to consider such less complex models, at least because they allow to study the dependence of model properties on the input data without limitations due to computer capacity.

The main goal of the present paper is the confrontation of the predictions of such hybrid models with a large set of observational constraints. In addition to a "minimal set" (Prantzos & Aubert 1995) we consider further constraints like the rates for both types of SNe, the luminosity function of white dwarfs (WDLF) and the present-day mass function of main-sequence stars (PDMF) in the solar vicinity.

Gas inflow via viscous transport may play an important role for the evolution of the central regions of disks (Courthau et al. 1996). Viscous evolution results in a radial stellar density distribution which is exponential over several scalelengths. In the innermost region ($R < 1...3$ kpc), the stellar density increases much stronger. It has been suggested to identify this surplus of mass with the Galactic bulge (Yoshii & Rodgers 1989; Weinberg 1992; Tsujimoto et al. 1995 a). We will examine this hypothesis in the framework of our models.

The paper is organised as follows: The general procedure, the set of equations and assumptions, and the fundamental ingredients of the models are described in the next section. In Sect. 3, we present a summary of the observational constraints, inclusive of a brief discussion of the observed abundance gradients and indications for their evolution. The results from an extended parameter study of viscous models are presented in Sect. 4, along with the analysis of "best-fit" models. The inner part of the disk is discussed separately in Sect. 5. Conclusions are given in Sect. 6.

2. The basics of the models

2.1. General description

The main properties of the models are described as follows:

We proceed from the assumption that the early evolution of the Galactic disk is widely affected by infall of dissipated gas from the protogalactic halo, and that the infall continues to influence the evolution on longer timescales, especially in the outer regions of the disk. The evolution in the differentially rotating disk is determined by star formation, viscosity of the gas, and infall of external gas.

Following Lin & Pringle (1987) we assume that the viscosity in the gas is closely related to the processes of star formation and the energetic response from young stars. On the basis of such a tight relation, the star formation rate (SFR) is derived from the prescribed viscosity law. Because of the lack of a theory we describe the viscosity by a very simple, general parametrisation. The disk gas is enriched with Fe and O by SNe of the types Ia and II.

The models are one-dimensional, i.e. we integrate over the vertical structure of the disk. We assume efficient azimuthal chemical mixing of the interstellar medium (ISM) in the sense that we neglect azimuthal structures like spiral arms (e.g., Martin & Belley 1996). We allow, however, for chemical inhomogeneities in the ISM of the same given Galactocentric distance at any given time. The calculations do not use the common instantaneous recycling approximation (IRA).

2.2. Basic equations

2.2.1. Balance equations

We describe the evolution with time t of the gas density Σ_g, the stellar density Σ_*, and the mass fraction Z of a chemical element in the ISM in dependence on the galactocentric radius R:

$$\frac{\partial \Sigma_g}{\partial t} = I - \Psi_{net} - \frac{1}{R}\frac{\partial}{\partial R}\Big(R\Sigma_g v_R\Big), \quad (1)$$

$$\frac{\partial \Sigma_*}{\partial t} = \Psi_{net}, \quad (2)$$

$$\frac{\partial (Z\Sigma_g)}{\partial t} = P_{net} + F_{net} + IZ^{inf}. \quad (3)$$

Eqs. (1) to (3) are the balance equations. The terms on the right hand side of Eq. (1) describe (from left to right) gas infall, the net gas consumption by star formation, and the radial gas flow, respectively, where v_R is the radial velocity of the radial gas flow. The terms in Eq. (3) are the net-effects to the heavy-element enrichment by stellar evolution (P_{net}), viscous radial gas flow and viscous diffusion (F_{net}), and gas infall (IZ^{inf}), respectively. I is the infall rate ($m_\odot$ Gyr^{-1} pc^{-2}), Z^{inf} is the mass fraction of the corresponding chemical element in the infalling gas. All relevant densities are column densities ($m_\odot$ pc^{-2}). All functions depend on R and t.

The net-effect of star formation for the gas balance is described by the difference between the SFR Ψ ($m_\odot$ Gyr^{-1} pc^{-2}) and the integrated returned mass from all evolved stars which were born before

$$\Psi_{net} = \Psi - \int_{m_t}^{m_u} [1 - r_m]\Psi(t - \tau_m)\Phi(m)dm, \quad (4)$$

where $1 - r_m$ is the returned mass fraction of stars of the mass m, and τ_m is the lifetime of a star of mass m. $\Phi(m)\,dm$ is initial mass function (IMF), i.e.the mass fraction of newly formed stars in the dm interval around m, The "turn-off"-mass at age t and the upper stellar mass limit are denoted by m_t and m_u, respectively. Note that, throughout this paper, terms within parenthesis are arguments whereas terms within brackets indicate factors.

Element enrichment is driven by star formation due to the integrated ejection of the corresponding chemical element from all evolved stars

$$P_{net} = -Z\Psi + \int_{m_t}^{m_u} Q(m)\Psi(t - \tau_m)\Phi(m)dm, \quad (5)$$

where the mass fraction, $Q(m)$, of the elements returned to the ISM consists of two terms

$$Q(m) = [1 - r_m]Z(t - \tau_m) + P(m), \quad (6)$$

namely the fraction of the elements which was locked up in stars in the process of star formation and the fraction of mass, $P(m)$, of newly synthesised and ejected elements.

The term F_{net} in Eq. (3) is given by

$$F_{net} = \frac{1}{R}\frac{\partial}{\partial R}\Big(R\Sigma_g \nu \frac{\partial Z}{\partial R}\Big) - \frac{1}{R}\frac{\partial}{\partial R}\Big(R\Sigma_g v_R Z\Big). \quad (7)$$

The first term on the right-hand side is the standard diffusion term (cf. Sommer-Larsen & Yoshii 1990), where we adopted the diffusion coefficient to be equal to the viscosity coefficient, $\nu_D = \nu$. For a flat rotation curve this assumption is identical to Eq. 12 in Sommer-Larsen & Yoshii (1989). The second term describes the effect of the radial flow. The radial velocity of the flow v_R is obtained from the hydrodynamic transport equation:

$$\Sigma_g v_R\Big[\frac{\partial v_\phi}{\partial R} + \frac{v_\phi}{R}\Big] = \\ = \frac{1}{R^2}\frac{\partial}{\partial R}\Big(\Sigma_g \nu R^3 \frac{\partial}{\partial R}\frac{v_\phi}{R}\Big) + [v_\phi^{inf} - v_\phi]I - \Sigma_g \frac{\partial v_\phi}{\partial t}. \quad (8)$$

The first two terms reflect the radial flow induced by viscosity, and infall, respectively, where $v_\Phi(R)$ is the rotation curve and v_Φ^{inf} is the rotation velocity of the infalling gas at the radial position of the infall. The third term comes from a time-variable rotation curve. Eq. (8) is fully derived in the Appendix.

2.2.2. Viscosity and star formation rate

Following Lin & Pringle (1987), we assume that the viscosity in the gas is closely related to the processes of star formation and the energetic response from massive stars, i.e. the timescales for viscous transport, t_ν, and for gas consumption by star formation, t_*, are nearly the same:

$$\beta \equiv \frac{t_*}{t_\nu} = const. \approx 1. \quad (9)$$

This is what we call throughout this paper the "Lin-Pringle condition". Struck-Marcell (1991) has argued that the assumption of Eq. (9) corresponds to a steady-state hydrodynamic equilibrium of the Galactic disk. The star formation timescale is defined by

$$t_* = \frac{\Sigma_g}{\Psi}, \quad (10)$$

and the viscous timescale is given by (Pringle 1981)

$$t_\nu = \frac{R^2}{\nu}. \quad (11)$$

From Sommer-Larsen & Yoshii (1989) we adopt the parametrization of the viscosity:

$$\nu = \nu_0 \Sigma_g^a R^b, \qquad \nu_0, a, b = const. \quad (12)$$

Thus, the SFR is obtained from the combination of the Eqs. (9) to (12):

$$\Psi = \frac{\nu_0}{\beta}\Sigma_g^{a+1} R^{b-2}. \quad (13)$$

It has been demonstrated (e.g., Olivier et al. 1991) that some frequently used descriptions of the SFR (Schmidt 1963; Kennicutt 1989; Wyse & Silk 1989) are realised by such a parametrization with $a = 0 \ldots 2$ and $b = 1 \ldots 3$.

2.2.3. Chemical enrichment due to SNe of type Ia

The modelling of the chemical enrichment due to SNe Ia follows the formulation by Greggio & Renzini (1983) and Matteucci & Greggio (1986) for degenerated white dwarfs in symbiotic binaries. The fraction of such systems is scaled in the model by a further free parameter A. In modification of the source term in the integral on the right-hand-side of Eq. (5), the contribution of enrichment due to SNe Ia is described by

$$A \int_{m_{B,inf}}^{m_{B,max}} \Phi(m_B) P_1(m_B) \int_{\mu_{inf}}^{0.5} f(\mu)\Psi(t-\tau_{m2}) d\mu\, dm_B, \quad (14)$$

where $P_1(m_B)$ is the mass fraction of the corresponding chemical element newly synthesized and ejected by a SN Ia in a binary of the mass m_B which has to be within the range between $m_{B,min} = 3\,m_\odot$ and $m_{B,max} = 16 m_\odot$. For evolved stages of a stellar system, the lower integration limit $m_{B,inf}$ is determined by the turn-off mass $m_t(t)$, so $m_{B,inf} = \max[2m_t(t), m_{B,min}]$. The mass fraction of the secondary component of the binary, $\mu = m_2/m_B$, has the distribution $f(\mu)$ with a lower limit set by $\mu_{inf} = \max[m_t(t)/m_B, (m_B - 0.5 m_{B,max})/m_B]$ (see Greggio & Renzini 1983).

2.2.4. Gas infall

Infall of primordial gas was incorporated following Sommer-Larsen & Yoshii (1990):

$$I = \frac{I_0\, \Sigma_0^i(R)}{t_i} e^{-t/t_i}; \qquad t_i(R) = t_i(R_\odot)\frac{R}{R_\odot}, \quad (15)$$

where $\Sigma_0^i(R)$ describes the radial gas density profile of the infalling gas (see Sect. 2.3). If not stated otherwise, we assume $\Sigma_0^i = \Sigma_0$, where Σ_0 is the initial gas density profile (see Sect. 2.4). The free parameter I_0 regulates the total mass fraction, i, of the infalling gas

$$i = \frac{2\pi}{m_{tot,1}} \int_{t=0}^{t_1} \int_{R=0}^{\infty} I\, R\, dR\, dt, \quad (16)$$

where $m_{tot,1}$ is the total mass (in $m_\odot$) of the model galaxy at the present age, t_1, of the Galactic disk. Sommer-Larsen & Yoshii found a good fit to the observed metallicity distribution of G dwarfs for an infall timescale at the solar position $t_i(R_\odot) = 6.4$ Gyr.

2.2.5. Numerical method

The model equations (1) to (3) were solved, in combination with the relations (4) to (8) and (12) to (15), using a first order forward-time-centred-space scheme (FTCS). Such a procedure requires a much higher grid resolution in time than in space to maintain stability and accuracy, but preserves the physical structure of the equations, what is most important for error detection. The calculations cover a radial range from $R = 0$

to 40 kpc which is divided into 100 equally spaced cells of $\Delta R = 0.4$ kpc. The timespan for disk evolution is assumed to be 12 Gyr (Sect. 3) and is resolved into 10^5 timesteps leading to $\Delta t = 1.2\,10^{-4}$ Gyr. The fixing of Δt results as a compromise between overall stability and accuracy of the numerical scheme, on the one hand, and acceptable calculation times, on the other hand. The computation time for one model is typically about 2 hours on a SUN ULTRA 1Cm170E workstation.

2.3. Approximations

In most previous studies of viscous disks, chemical evolution was simplified by the use of the IRA, i.e. the assumption that gas from evolved stars is returned into the ISM immediately after star formation. This is a good approximation for chemical evolution if chemical elements are considered which are synthesized in massive stars, and, furthermore, if the mass fraction of the gaseous component does not fall much below 0.1. When modelling radial abundance gradients, neither of these conditions is realised (cf. Prantzos & Aubert 1995). As test calculations revealed considerable differences for the results from IRA and non-IRA calculations of the same model we decided not to apply the IRA. The radial abundance gradients are, in general, reduced when relaxing the IRA.

We assume a flat rotation curve with $v_\Phi = 220$ km/s. The observed flat outer rotation curves of disk galaxies are generally explained by extended dark matter halos. In the inner disk, however, the gravitational potential of the disk could outweigh the dark halo. The evolution of the mass distribution due to gas infall as well as due to the radial gas drift changes the inner rotation curve, which has, in turn, a retroactive effect on the gas drift itself. It is not *a priori* clear that a constant rotation curve is a good approximation in galaxy evolution models with changing mass profiles, especially with respect to the strong radial gas flows occurring in the innermost part of our model disks. We examined the self-consistent evolution of the disk with a rotation curve given by $v_\phi(R;t) = \sqrt{Gm(R;t)/R}$, where $m(R;t)$ is the total mass inside R, consisting of disk, bulge+halo, and extended dark matter halo, G is the gravitation constant. The radial gas drift was found to generate quickly a flat inner rotation curve to the same degree as the exponential disk density profile is build up. A similar result was reported by Saio & Yoshii (1990). The fact that the disk rotation velocity in the inner disk is adapted to the value preset by the dark halo is a further attractive property of the viscous models. As a practical consequence, the assumption of a simple rotation curve that is constant in time and space is, in general, a reliable approximation (Fig. 1).

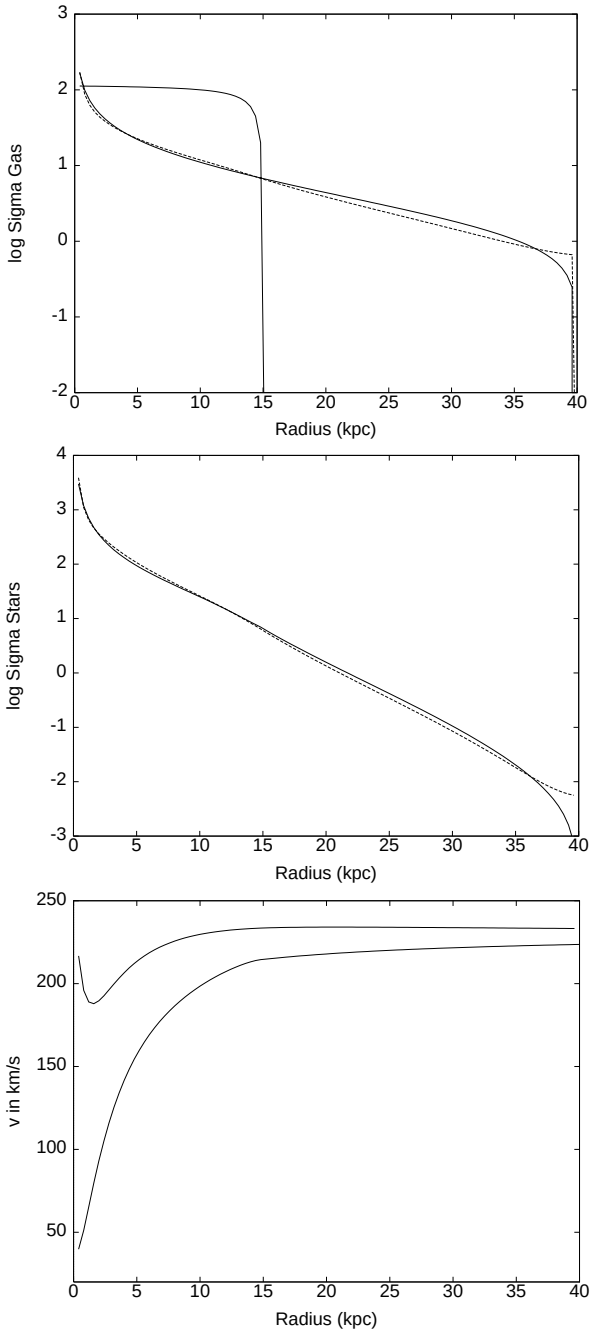

Fig. 1. Effects of a variable rotation curve. Resulting ($t = t_1$) radial gas density profile (*top*) and stellar density profile (*middle*) for models with a variable (dotted) and a constant (strong) rotation curve. Densities are in $m_\odot$ pc^{-2}. (In the top panel, also the initial gas density profile is shown by the curve truncated at 15 kpc.) *Bottom*: Initial (lower) and final ($t = t_1$, upper) rotation curve, respectively. There was no initial bulge adopted in this model.

2.4. Initial and boundary conditions

We adopted different radial gas distributions for the initial disk. It has been suggested by several authors (e.g., Yoshii & Sommer-Larsen 1989; Sommer-Larsen & Yoshii 1989, 1990; Olivier et al. 1991) that the radial surface density profile of the initial gas disk should be that of a truncated isothermal sphere with a ratio of core radius to truncation radius of 0.42. In the present paper, this density profile is considered as the standard initial profile with a truncation radius of 15 kpc, corresponding to 5 stellar scalelengths or approximately the Holmberg radius (Olivier et al. 1991). Alternatively, we consider either an exponential profile or a profile of the form $\Sigma_g(R) \propto \sqrt{(const. - R)}/R$ which follows from the disk formation scenario by Gunn (1982).

Both zero-torque ($\Sigma_g = 0$) and zero-flux ($v_R = 0$) inner and outer boundary conditions were used. The outer boundary condition has no remarkable effect on the disk evolution if its radius is sufficiently large (i.e. 10 scalelengths). The zero-flux boundary condition leads to an increased central accumulation (cf. Clarke 1989). In most models we used zero-torque inner and outer boundary conditions.

2.5. Further ingredients of the models

Besides the SFR, the IMF is one of the most fundamental key functions of the models. The IMF is conventionally described by a time-invariant power-law $n(m) \propto m^{-(1+x)}$, where $n(m)\,dm$ denotes the number of stars in the mass interval $m...m+dm$ (Salpeter 1955: $x = 1.35$). We adopted the IMF from Kroupa et al. (1993) where a detailed model of star-count data was developed in which selection effects were consistently taken into account. In the notation of the present paper, the IMF is $\Phi(m) \propto m^{-x_i}$ with

$x_1 = 0.3\ (-0.3...0.85)$ for $0.08 < m/m_\odot \leq 0.5$
$x_2 = 1.2$ for $0.5 < m/m_\odot \leq 1.0$
$x_3 = 1.6$ for $1 < m/m_\odot$,

where the slope x_3 for $m > 1\,m_\odot$ is based on the Scalo (1986) IMF. The flattening of the IMF towards low-mass stars is also indicated by star counts in star clusters (e.g., De Marchi & Paresce 1997; Meusinger et al. 1996). A comparison with other recent results on the IMF is presented by Kroupa (1997). A new approach for constraining the IMF parameters arises from SN nucleosynthesis data in combination with observed heavy-element abundance ratios (Wyse & Gilmore 1992; Tsujimoto et al. 1997). In Sect. 3.4 we will consider the consistency of the IMF with the SN nucleosynthesis data.

The oxygen and iron enrichment of the ISM occurs exclusively by SNe. We adopted the production rates for SNe II either from Tsujimoto et al. (1995 b) or from Woosley & Weaver (1995, model type SA, respectively SB where there is such a choice) and for SNe Ia from Tsujimoto et al. (1995 b). The chemical element mass fractions Z predicted by the model were transformed into abundance ratios $[O/H]$ and $[Fe/H]$, respectively, adopting the solar abundance data from Grevesse & Anders (1989).

The distribution function of the mass fraction of the secondary component in binaries, $f(\mu)$, is needed to compute the element enrichment by SNe Ia (Eq. 14). A simple formulation of $f(\mu)$ was quoted by Greggio & Renzini (1983) and Matteucci & Greggio (1986). Duquennoy & Mayor (1991) derived the frequency distribution of mass ratios from a detailed investigation of the nearby double stars. Although both relations are different (unlike the former relation, the latter one does not show a maximum at $\mu = 0.5$), the differences in the model results are not very large. We adopted the relation given by Greggio & Renzini for the parameter study (Sect. 4.1). For the search of best-fit models (Sect. 4.2) , however, we used $f(\mu)$ from the Duquennoy & Mayor (1991) data.

The stellar mass-lifetime relation $\tau(m)$ was constructed from a combination of stellar models by VandenBerg (1985) for $m \leq 3m_\odot$ and by Schaller et al. (1992) for $m > 3m_\odot$. The initial-final mass relation was taken from Weidemann (1987) and Koester & Reimers (1996) for $m \lesssim 10\,m_\odot$, from Woosley & Weaver (1995) for $12 \leq m/m_\odot \leq 60$, and from Maeder (1992) for $m > 60m_\odot$.

The model WDLF and PDMF were calculated following the procedure outlined e.g. by Yuan (1992). White dwarf cooling times from Wood (1992) were used to calculate the WDLF. The resulting white dwarf surface densities were transformed to volume-related data adopting the empirical scaleheight-age relation for Miras (Wyatt & Cahn 1982) which are supposed to be the progenitors of white dwarfs (cf. Isern et al. 1997).

A disk age of $t_1 = 12$ Gyr was adopted because this seems the best compromise for the age data from open clusters, field F and G main sequence stars, and white dwarfs (Majewski et al. 1997; Isern et al. 1997; Meusinger 1994). Alternatively, we have also computed a large set of models with $t_1 = 15$ Gyr; the general model properties do not significantly depend on t_1.

The position of the Sun is assumed at $R_\odot = 8.5$ kpc.

3. Observational constraints from the Galactic disk

The whole set of observational constraints confronted with the model predictions is listed in Tables 1 and 2. Some of these constraints are discussed below in more details: the abundance distribution of G dwarfs, the age-metallicity relation, the $[O/Fe]$–$[Fe/H]$ relation, and the radial abundance gradients. The radial density distributions have been discussed in more detail by Prantzos & Aubert (1995). A "minimal set" of observables (cf. Prantzos & Aubert 1995) is shown in Figs. 5 and 6.

3.1. Abundance distribution of the nearby long-lived stars

The abundance distribution function (ADF) of the long-lived stars is one of the most severe local constraints for chemical evolution models of the Galactic disk (van den Bergh 1962; Schmidt 1963; Pagel & Patchett 1975; Pagel 1989). The observational data have become significantly improved by the work of Wyse & Gilmore (1995) and Rocha-Pinto and Maciel (1996), respectively. These new data do not relaxe the classical "G dwarf problem", i.e. the prediction of too a high number of low-metallicity long-lived stars by simple evolution models. It seems unlikely that the G dwarf problem is simply due to selection effects in the stellar sample or of metallicity-dependent stellar lifetimes (Rocha-Pinto & Maciel 1997; Meusinger & Stecklum 1992).

The ADF presented by Rocha-Pinto & Maciel (1996) shows a pronounced peak around $[Fe/H] = -0.2$. On the other hand, Wyse & Gilmore (1995) emphasized that their $[Fe/H]$-distribution does not differ radically from earlier determinations. Differences between these both empirical ADFs may partly be due to different corrections for observational uncertainties. Wyse & Gilmore directly integrated over the solar cylinder by combining a local stellar sample with a distant one and deconvolved the abundance distribution into thin disk and thick disk components. However, as the peak is present also in the uncorrected data by Rocha-Pinto & Maciel, its different strength

Table 1. Set of observational constraints from the local Galactic disk.

	source	remark
ADF	Wyse & Gilmore (1995); Rocha-Pinto & Maciel (1996)	see Sect. 3.1
AMR	Edvardsson et al. (1993); Meusinger et al. (1991)	see Sect. 3.2
abundance scatter	Edvardsson et al. (1993)	see Sect. 3.3
$[O/Fe]\ vs.\ [Fe/H]$	Barbuy & Erdelyi-Mendes (1989); Edvardsson et al. (1993)	see Sect. 3.4
$\Psi(t_1)$	Rana (1991) and ref.s therein	$\approx 2...5\, m_\odot\ \mathrm{pc}^{-2}$
$b(t_1)$	Scalo (1986); Meusinger (1994)	$\approx 1\ (0.3...2)$
$\Sigma_g(t_1)$	Boulares (1989)	$\approx 14\, m_\odot\ \mathrm{pc}^{-2}$
$\Sigma_*(t_1)$	Gilmore et al. (1990)	$\approx 35 \pm 5\, m_\odot\ \mathrm{pc}^{-2}$
$PDMF$	Scalo (1986);	"standard" for $m > 1\, m_\odot$
	Basu & Rana (1992);	various corrections
	Kroupa et al. (1993);	low masses
$WDLF$	Liebert et al. (1988); Evans (1992)	various completeness corrections

$b(t_1) = \Psi(t_1)/\bar{\Psi}$: relative SFR, where $\bar{\Psi}$ is the average SFR;

Table 2. Set of global observational constraints from the Galactic disk.

	source	remark
$M_{tot;disk}$	Bahcall et al. (1982)	$\approx 5\,10^{10}\,\mathrm{m}_\odot$
$\Sigma_g(R;t_1)$	Dame (1993)	
l_*	van der Kruit (1989)	$= 3...4\,\mathrm{kpc}$
$\Psi(R;t_1)/\Psi(R_\odot;t_1)$	Lacy & Fall (1985) and ref.s therein	from H II-regions, pulsars, SN remnants
$d[Fe/H]/dR$	see 3.3	$\approx -0.08 \pm 0.03$ für $\tau < 5\,\mathrm{Gyr}$, $R \approx 5...13\,\mathrm{kpc}$
		$\approx -0.01 \pm 0.01$ für $\tau > 10\,\mathrm{Gyr}$, $R \approx 5...13\,\mathrm{kpc}$
$d[O/H]/dR$	see 3.3	$\approx -0.05 \pm 0.02$ für $\tau < 1\,\mathrm{Gyr}$, $R \approx 5...13\,\mathrm{kpc}$
R_{SN}	Tammann et al. (1994); Muller et al. (1992);	$\approx 1...5\,10^{-2}\,\mathrm{yr}$
	Cappellaro et al. (1993)	where $R_{SNIa}/R_{SNII} \approx 0.2$
$I(t_1)$		$\lesssim 1\,\mathrm{m}_\odot\ \mathrm{pc}^{-2}\,\mathrm{Gyr}^{-1}$
	Wakker & van Woerden (1991):	high velocity H I clouds
	Briggs (1990)	extragalactic gas ressources
$v_\phi(R)$	e.g., Burton (1992)	$\approx 220\,\mathrm{km\,s}^{-1} \approx const$

$m_{tot;disk}$: total mass of the disk; l_*: scalelength of the exponential stellar density profile; $\Psi(R;t_1)/\Psi(R_\odot;t_1)$: normalized radial profile of the present-day SFR; R_{SN}: SN rate; $I(t_1)$: present-day gas infall rate; $v_\phi(R)$: rotation curve.

is perhaps due to different stellar samples rather than due to different data corrections.

We compare the model $[Fe/H]$-distribution of long-lived stars with the observed ADF from Rocha-Pinto & Maciel, as well as with the combined thin+thick disk distribution from Wyse & Gilmore. In the latter case, we take into account that the models do not distinguish between thick disk and thin disk, and that these both components may be the product of a uniform formation process (e.g., Majewski 1993; Wyse & Gilmore 1995).

3.2. The age-metallicity relation (AMR) of the local disk

Empirical studies on ages and metallicities of stars in the solar neighbourhood have established the idea that the heavy element abundances in the ISM, averaged over suitable temporal and spatial regions, have slightly increased in the course of the evolution of the local Galactic disk (Mayor 1976; Twarog 1980; Carlberg et al. 1985; Schuster & Nissen 1989; Meusinger et al. 1991; Edvardsson et al. 1993). On the basis of Strömgren photometric data for nearly 5 000 disk dwarfs, Twarog (1980) created a well-defined sample of about 900 F and G dwarfs to derive the AMR. A re-analysis of this photometric data base was presented by Meusinger et al. (1991) using revised calibrations of the photometric indices, updated stellar evolution models, and a

more elaborated method of age determination. Nevertheless, the resulting AMR was quite similar to that found by Twarog. Edvardsson et al. (1993) presented very precise abundance data for nearly 200 nearby F and G dwarfs which provide a very suited data base for studying chemical properties of the Galactic disk. The AMR derived for the stars representing the solar cylinder ring (7.7 kpc$< R_m <$ 9.3 kpc, $|z_{max}| <$ 0.26 kpc, $e <$ 0.11) is in good agreement with the previously derived AMRs for the solar neighbourhood, too. The data point for the oldest stars may be slightly biased toward lower matallicities (Edvardsson et al. 1993).

In the present paper, we will confront our model AMR with the AMRs from Edvardsson et al. and Meusinger et al. (Figs. 5 to 8). The age bin for the oldest stars in the latter AMR is much in excess of 12 Gyr. To maintain consisteny with the adopted disk age we decided to scale down the ages in this AMR by a factor 0.8. This may be an oversimplification. However, simulations have shown (Meusinger 1994) that a disk age of about 15 Gyr may be pretended by the age distribution of the stellar AMR sample even if the true age is only about 12 Gyr, simply due to the uncertainties of age determination.

3.3. Abundance scatter

It is a well-known property of the AMR to show a considerable abundance scatter among stars born at the same time at the same Galactocentric distance. Twarog (1980) found a dispersion of $\sigma_{[Fe/H]} = 0.12$ dex, nearly in agreement with the expected uncertainty of the abundance determination. A somewhat larger dispersion was present in the revised AMR by Meusinger et al. (1991), ranging from 0.13 dex for stars younger than 2 Gyr to 0.24 dex for the oldest stars. Large abundance variations are also indicated by similarly aged open clusters after correction for the radial abundance gradients across the Galactic plane (e.g., Carraro & Chiosi 1994; Piatti et al. 1995). The accurate data presented by Edvardsson et al. (1993) have clearly demonstrated that the observed abundance scatter at fixed age is much larger than that expected from observational uncertainties assumed as about 0.05 dex. After correction for the kinematic evolution perpendicular to the Galactic plane $\sigma_{[Fe/H]}$ seems to increase with age from about 0.15 to about 0.25 (Wielen et al. 1996).

The relation between metallicity dispersion and age has been interpreted by Wielen et al. (1996) as confirmation of the hypothesis of stellar orbital diffusion, predicted already by Wielen (1977). Van den Hoek & de Jong (1997) have argued that diffusion of stellar orbits is probably insufficient to explain the observed abundance scatter. Alternative ideas include self-enrichment in regions of sequential star formation (Edmunds 1975), irregular infall of unenriched gas onto the disk (Pilyugin & Edmunds 1996), or a combination of both (van den Hoek & de Jong 1997).

In the present paper, we do not follow in detail the possible processes causing the abundance inhomogeneity in the Galactic disk. However, we have to take into account the abundance scatter when comparing the model ADF with the empirical G dwarf distribution: Following Pagel (1989), Rocha-Pinto & Maciel (1996) have deconvolved the observed ADF with a Gaussian of dispersion $\sigma_{[Fe/H]} = 0.1$ to correct for the uncertainties in the abundance determination. In order to account for a further "cosmic" scatter, expressed by $\sigma_{[Fe/H],c}$, we convolve the model ADF with a Gaussian with the dispersion $\sigma_{[Fe/H],c} = 0.1 + 0.1\tau/t_1$, where τ is the age. Because the effect of erroneous age determinations on the abundance scatter at fixed age is difficult to estimate, we will alternatively consider the case $\sigma_{[Fe/H],c} = 0.1 = const.$ Malinie et al. (1993) have shown that the fit to the empirical ADF is improved in a model of inhomogeneous chemical evolution, especially at the high metallicity end of the ADF.

3.4. $[O/Fe]$ $vs.$ $[Fe/H]$ relation

The dependence of the abundance ratio $[\alpha/Fe]$ for α elements on $[Fe/H]$ is generally interpreted as due to different lifetimes of the main producers of the different elements. Especially, the $[O/Fe]$ $vs.$ $[Fe/H]$ relation is explained by the long lifetimes of progenitors of SNe Ia responsible for iron enrichment compared to those of SNe II driving the oxygen evolution (e.g., Matteucci & Francois 1989). The observed ratio $[O/Fe] \approx 0.5$ for $[Fe/H] < -1$ can be explained as exlusively originating from SN II enrichment, while the slope of the $[O/Fe]$–$[Fe/H]$ relation for $[Fe/H] > -1$ (Edvardsson et al. 1993) depends on the ratio of the SN II to SN Ia rates, i.e. on the slope of the IMF for $m > 1\,m_\odot$.

Therefore, we determined the IMF index x_3 by making the demand to reproduce the observed slope $d[O/Fe]/d[Fe/H] \approx -0.5$ for $[Fe/H] \gtrsim -1$. On the other hand, the maximum stellar mass, $m_{max,SN\,II}$, contributing to the ISM enrichment via SNe II, i.e. the mass limit beyond which stars end as black holes without ejecting processed matter into the ISM, has mainly the effect of shifting the $[O/Fe]$-$[Fe/H]$ relation along the $[O/Fe]$ axis (cf. Tsujimoto et al. 1995 a). Once x_3 is specified, we found $m_{max,SN\,II}$ by fitting $[O/Fe]$ at $[Fe/H] \approx -1$. For the SN II element production rates from Tsujimoto et al. (1995 b) we find a good agreement with the observed $[O/Fe]$–$[Fe/H]$ relation assuming $x_3 = 1.6$ and $m_{max,SN\,II} = 60\,m_\odot$ (Fig. 2). The use of the metallicity-dependent SN II yields from Woosley & Weaver (1995), however, does not result in a flattening of $[O/Fe]$ at low metallicities. For the search of best-fit models (Sect. 4.2) we restrict our analysis to the data from Tsujimoto et al. (1995 b). In a more detailed investigation of a similar approach, Tsujimoto et al. (1997) found $x_3 = 1.3...1.6$ and $m_{max,SN\,II} = 50 \pm 10\,m_\odot$.

3.5. Radial abundance gradients (RAGs)

Although there are strong indications for the existence of overall radial heavy element abundance gradients in our Galaxy, the values for the gradients are still a matter of debate. From a comprehensive analysis of H II regions, Shaver et al. (1983) found a strong RAG of $d[O/H]/dR = -0.07$ dex kpc^{-1} (for $R_\odot = 10$ kpc). Over the last years, abundances have been estimated for distant B stars and H II regions by several groups. The results are listed in Table 3, together with RAGs derived from

Table 3. Radial abundance gradients in the Galaktic disk.

R ($R_\odot$)	age (Gyr)	object group	$d[O/H]/dR$ (dex/kpc)	$d[Fe/H]/dR$ (dex/kpc)	references
4...11	0	diffuse H II regions	-0.079 ± 0.020		Shaver et al. (1983)
4...11	0	ultra compact H II regions	-0.047 ± 0.009		Afflerbach et al (1996)
4...11	0	compact H II regions	-0.054 ± 0.018		Afflerbach et al. (1997)
6...13	< 0.1	B stars	-0.03 ± 0.02		Fitzsimmons et al. (1992)
5...10	< 0.1	B stars	-0.035 ± 0.021	-0.054 ± 0.036	Kilian-Montenbruck et al. (1994)
6...18	< 0.1	B stars	-0.07 ± 0.01		Smartt & Rolleston (1997)
4...8.5	< 0.1	B stars	-0.03 ± 0.3		Smartt et al. (1997)
	0.1	open clusters	-0.07		Janes et al. (1988)
6...13	0.2	open clusters		-0.06 ± 0.01	Piatti et al. (1995)
6...13	1	open clusters		-0.07 ± 0.01	Piatti et al. (1995)
4...15	1 ± 1	PN I	-0.030 ± 0.007		Maciel & Köppen (1994)
6...11	2.9 ± 2	F,G dwarfs		-0.113 ± 0.008	Edvardsson et al. (1993)
4...12	5 ± 3	PN I,II	-0.03		Pasquali & Perinotto (1993)
7...16	3.1 ± 2.2	open clusters		-0.097 ± 0.017	Thorgensen et al. (1993)
4...15	5 ± 1	PN II	-0.069 ± 0.006		Maciel & Köppen (1994)
4...15	9 ± 1	PN III	-0.058 ± 0.008		Maciel & Köppen (1994)
4...17	10 ± 3	K giants		-0.018 ± 0.001	Lewis & Freeman (1989)
4...12	13.3 ± 2	F,G dwarfs		$+0.002 \pm 0.02$	Edvardsson et al. (1993)
2...8	12.5 ± 2.5	disk globular clusters		-0.022 ± 0.01	Alfaro et al. (1993)

planetary nebulae, disk globular clusters, field stars, and photometric abundances in open clusters. The RAG quoted there for the study by Shaver et al. was obtained from the well-determined abundances (their Eq. 13 a) after scale change to $R_\odot = 8.5$ kpc. The RAG from Smartt et al. (1997) is estimated from the average $[O/H]$ for four blue supergiants at $R_g \approx 4$ kpc derived by Smartt et al. compared with solar abundance at $R_\odot$. In the most studies quoted in Table 3, $R_\odot = 8.5$ kpc was adopted. Pasquali & Perinotto (1993) and Edvardsson et al. (1993), respectively, used slightly different values for $R_\odot$ which do not influence the estimated RAGs. The RAG for the K giants studied by Lewis & Freeman (1989) was corrected by Sommer-Larsen & Yoshii (1989) for the vertical abundance gradient. The corresponding value quoted in Table 3 was derived from these corrected data for the R range given in the Table. The $[Fe/H]$ gradients for the F and G dwarfs have been calculated from the abundance data and the mean Galactocentric distances, R_m, given by Edvardsson et al. (1993; their Tables 11 and 12).

Kaufer et al. (1994) and Vílchez & Esteban (1996) have pointed out that the RAGs are becoming shallower at larger R and are vanishing in the outermost part of the disk. The assumption of a linear RAG over the whole disk may be too simple. Therefore, we have recalculated the RAG for the compact H II regions from Table 3 in Afflerbach et al. (1997) using only objects with $R \geq 4$ kpc, in order to have a comparable R range.

The results in Table 3 confirm the existence of a radial $[O/H]$ gradient, partly however with a significantly lower slope than found by Shaver et al. (1983). As a compromise for all data in Table 3, a RAG of about $d[O/H]/dR = -0.05 \pm 0.02$ dex kpc^{-1} seems representative for the present-day ISM in the range $R \approx 4...11$ kpc. Kennicutt & Garnett (1996) found $d[O/H]/dR = -0.04...-0.05$ dex kpc^{-1} for the disk of M 101 at $R \approx 7.5$ kpc.

There are weak indications for a steepening of RAGs during the evolution of the disk (Table 3). Maciel & Köppen (1994) discussed a possible age-dependence in the RAGs from planetary nebulae data, although no individual age determinations are available. The mean ages listed in Table 3 were taken from the original papers for the most object groups. For the disk globulars we simply adopted the limits of globular cluster ages derived by Jimenez et al. (1996). The mean age of the K giants from Lewis & Freeman (1989) was roughly estimated from the mean $[Fe/H]$ and the mean kinematic data using the AMR from Sect. 3.2 and the age-velocity dispersion relation from Wielen (1977). The nearby F and G dwarfs studied by Edvardsson et al. (1993) are also well-suited for studying the evolution of the RAGs because individual age data are available. For the 93 thin disk stars with ages $\tau < 5$ Gyr we find $d[Fe/H]/dR = -0.113 \pm 0.08$ dex kpc^{-1}, in contrast to $d[Fe/H]/dR = 0.002 \pm 0.002$ dex kpc^{-1} for the 43 stars with $\tau > 10$ Gyr. Vanishing RAGs are also indicated for field K giants (Lewis & Freeman 1989) and disk globular clusters (Alfaro et al. 1993).

For typical conditions in galaxy disks, the RAGs are, as a first approximation, not influenced by the diffusion of stellar orbits (Wielen et al. 1996). The alternative explanation for the small RAGs indicated by the older disk objects is that RAGs are generated in the course of the chemical evolution of the disk. However, one has to take into account the following: for the old stars abundances are related to iron-group elements

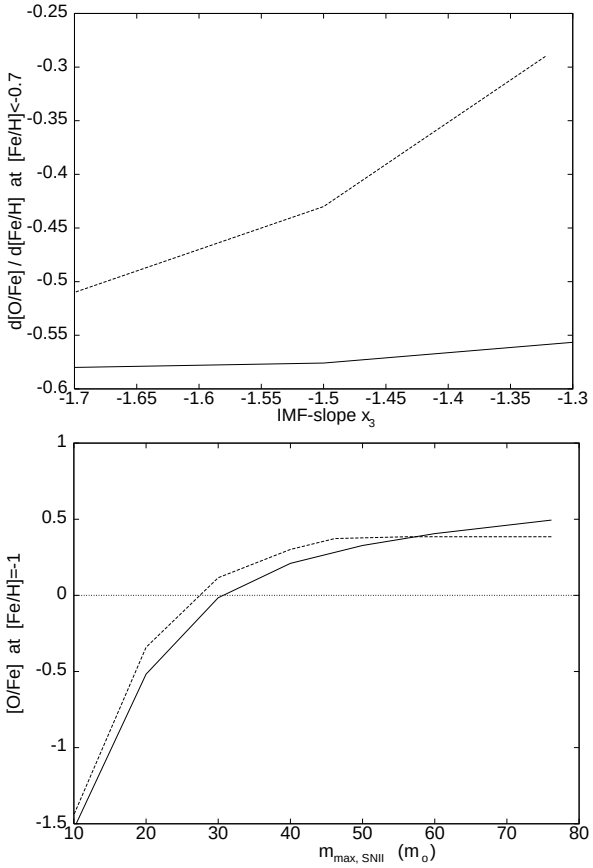

Fig. 2. *Top*: The slope of the $[O/Fe]\,vs\,[Fe/H]$ relation in dependence on the slope, x_3, of the IMF in the range $m > 1\,m_\odot$. *Bottom*: The element ratio $[O/Fe]$ at $[Fe/H] = -1$ as a function of the upper stellar mass contributing to the ISM enrichment via SN II for $x_3 = 1.6$. The solid curves are for the SN II yields from Tsujimoto et al. (1995 b), the dashed curves for the yields from Woosley & Weaver (1995).

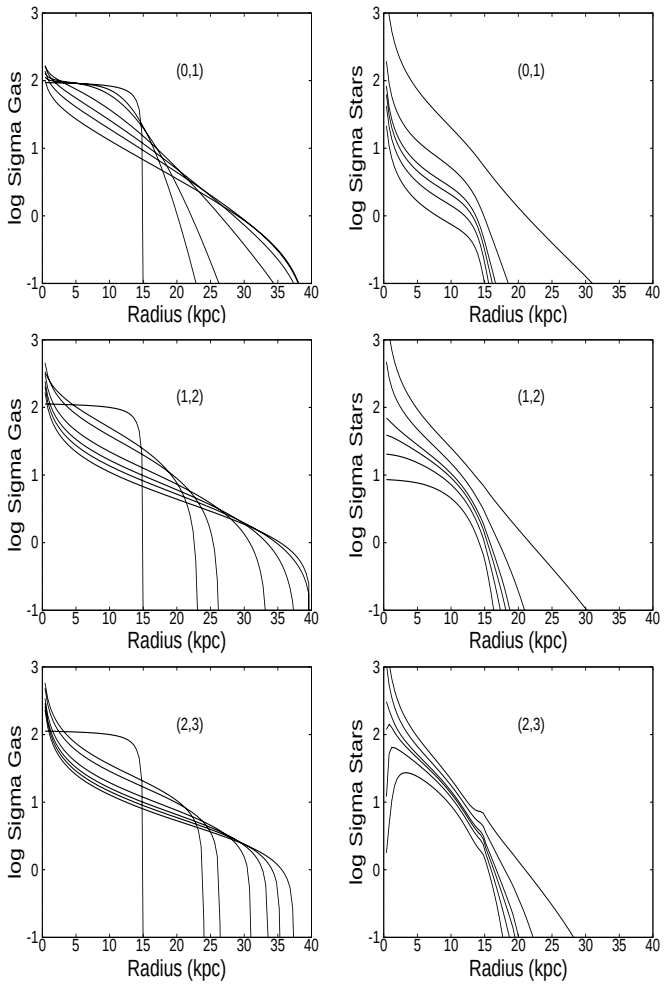

Fig. 3. The evolution of gas and star densities for $\beta = 0.5, i = 0$, and three different parameter sets (a, b) given in the panels. The time steps are 0, 0.015, 0.9, 3.0, 6.0, 9.0, 12.0, and 15.0 Gyr for the gas density profile and 0.15, 0.3, 0.45, 0.6, 1.5, 15.0 Gyr for the stellar density profile.

whereas young stars are related to oxygen. The empirical relation $[O/H] = c\,[Fe/H]$ with $c \approx 0.5$ is applicable for the nearby disk stars only, but not for the transformation between iron and oxygen RAGs. There is an interesting feature in the Edvardsson et al. data (cf. Nissen 1995): for $[Fe/H] < -0.4$ stars formed in the inner disk have a larger $[\alpha/Fe]$ than stars from the outer disk. With $d[O/H]/dR = d[O/Fe]/dR + d[Fe/H]/dR$ a formal gradient $d[O/Fe]/dR = -0.030$ dex kpc^{-1} implicates that the small gradient $d[Fe/H] = -0.01 \pm 0.01$ dex kpc^{-1} found for the old stellar population is nearly in agreement with the oxygen RAG. Nevertheless, there remains a difference between the $[Fe/H]$ gradient for the oldest and the younger stars, as indicated e.g. by the data from Edvardsson et al. (1993).

4. The viscously evolving Galactic disk

4.1. A parameter study of viscous models without infall

We performed model calculations for more than 3 500 different parameter combinations in order to examine general model properties for a broad range of parameters, and to limit the parameter space for the Galactic disk.

The general properties we found for the viscously evolving disks are largely in agreement with the results from previous studies (Clarke 1989; Sommer-Larsen & Yoshii 1989; Olivier et al. 1991): As a consequence of the radial gas flow, the system redistributes the initial gas density profile on a short timescale. The disk evolution is dominated by the flow for $\beta > 1$ and by the effects of star formation, respectively, if β is much less than 1, say $\beta \lesssim 0.1$. The stellar density profile generated in models with $\beta \approx 1$ is nearly exponential over a large fraction of the disk independent of the initial disk, whereas the resulting stellar scalelength, l_*, depends on the initial density profile. If the star formation timescale is short, the exponential stellar disk profile is forming quickly. As mentioned earlier (e.g. Simakov 1990; Fröhlich 1994), the evolution of the gas density profile (see Fig. 3) shows a remarkable self-similarity over about 90% of the disk age. The scalelength of the gaseous disk is generally longer than that of the stellar component.

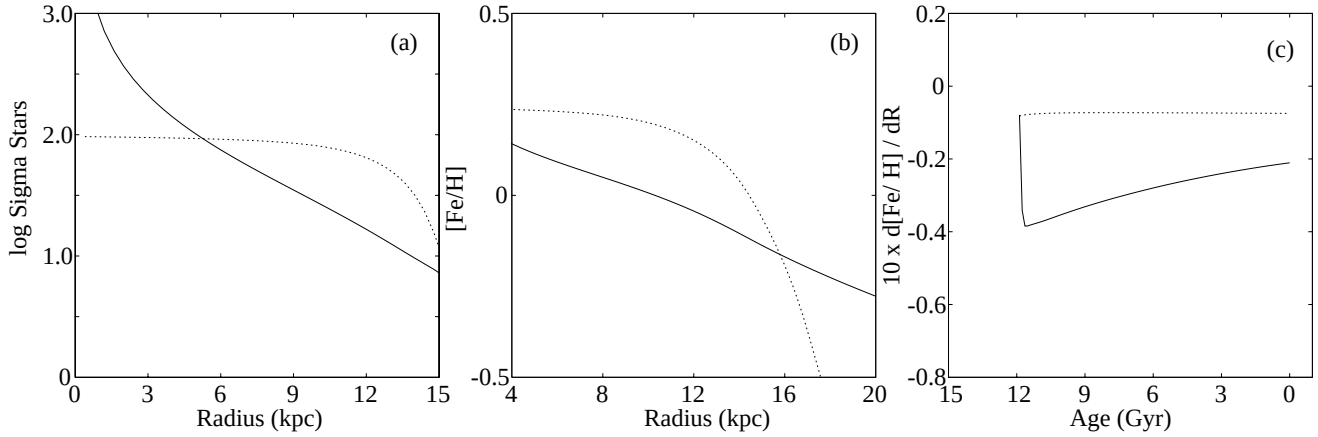

Fig. 4a–c. Effect of the viscous radial gas flow in models without infall. *Solid curve:* reference model $(a, b, \beta) = (1, 2, 0.5)$; *dotted curve:* the same model with strongly reduced viscosity, ν_0 (and correspondingly reduced β). The panels show (from left to right) **a** the radial stellar density distribution, **b** the radial iron abundance profile, and **c** the RAG for oxygen as a function of the age of star groups.

In the inner disk, the viscous flow is always directed toward the centre, in the outer region the gas flows outward. The inward-directed flow leads to an over-exponential central mass concentration along with a mass outflow through the inner boundary (for zero-torque boundary condition). A wide range of parameter values for the radial dependence of the viscosity is used in our study, in combination with different initial disk profiles. However, we could not find a model type for $\beta = 1$ where the central mass concentration becomes sufficiently suppressed whithout violating other observational constraints. Especially, models with $b - a \leq 0$ produce a less strong central stellar mass concentration as well as a flat final gas density profile for $R \lesssim 3$ kpc, but also too a flat gas density profile for $R \gtrsim 3$ kpc. Models with $b - a = 0$ are close to the observational limits for the gas density profile. There is only one way to reduce the central surplus mass and the mass outflow for otherwise good-fit models with a declining outer gas density profile: to reduce the viscosity, ν_0, and simultaneously the ratio $\beta = t_*/t_\nu$. Therefore, we adopt $\beta = 0.5$ for the most models considered below.

Due to the outward-directed gas flows the stellar density profile of an evolved disk is always smooth in the outer region (Fig. 3), even if the initial gas density profile was strictly truncated. Another consequence of the outward-directed flow is a very extended (about $10\, l_*$) gaseous disk with low densities in the outer part. In that context, extended gaseous disks of spiral galaxies (see Pfenniger et al. 1994, and references therein) may be interpreted as a result of viscous outflow rather than as a reservoir for star formation in the inner disk.

The effect of viscous flows on the evolution of RAGs is essentially twofold: The primary effect of the flow is the rapid radial redistribution of the gas leading quickly to a nearly exponential profile in the star formation rate, and therewith to RAGs. Stronger viscosity, i.e. a larger value for ν_0, leads to stronger concentration of the gas, and therewith of the SFR, towards the centre. The consequence is an increased RAG. On the other hand, the direct effect of the radial gas flow is to level radial abundance differences. This tendency is further enhanced by the effect of viscous diffusion (Eq. 7). For models starting from a flat initial gas density profile (e.g., our standard initial disk), the net effect of the radial gas flow is an amplification of the RAGs (Fig. 4a–c). In nearly all viscous models, RAGs are formed rapidly due to strong initial gas redistribution, but are slightly reduced or nearly constant with time for the most time of disk evolution. In general, the abundance profiles become shallower with increasing R. The gradients for the oldest stars are insignificantly larger for $[O/H]$ than for $[Fe/H]$.

4.2. "Best-fit" models with radial flows and infall

4.2.1. General

In this section, we consider such infall models with viscosity parameters $a = 0, 1, 2$, $b = 1, 2, 3$, $\beta = 0.5, 1$, and an infall mass fraction $i = 0.5$ to 0.95 which approximately reproduce the observational constraints in its entirety. Among the large number of models computed in the frame of this study, several models with different parameter sets were found to provide properties similar to that observed for the Galactic disk. This is what we call "best-fit" models. Because of the simple formulation of such model key functions as the SFR, it is not realistic to expect that any single model is able to reproduce all details of all constraints.

In particular, models with $b - a = 1$ can provide an acceptable fit to the whole set of empirical data. These parameter combinations (a, b) include the cases where viscosity and star formation are driven by cloud-cloud collisions ($a = 1,\ b = 2$) or gravitational instabilities ($a = 2, b = 3$), respectively (see Olivier et al. 1991). Properties of some best-fit models are listed in Table 4. A more detailed and more critical discussion follows below.

To save space, we restrict the demonstration of results to models with $(a, b) = (1, 2)$. Figs. 5 to 8 illustrate the predictions for different models with such parameters. The corresponding plots for models with $(a, b) = (0, 1)$ and $(2, 3)$ look quite simi-

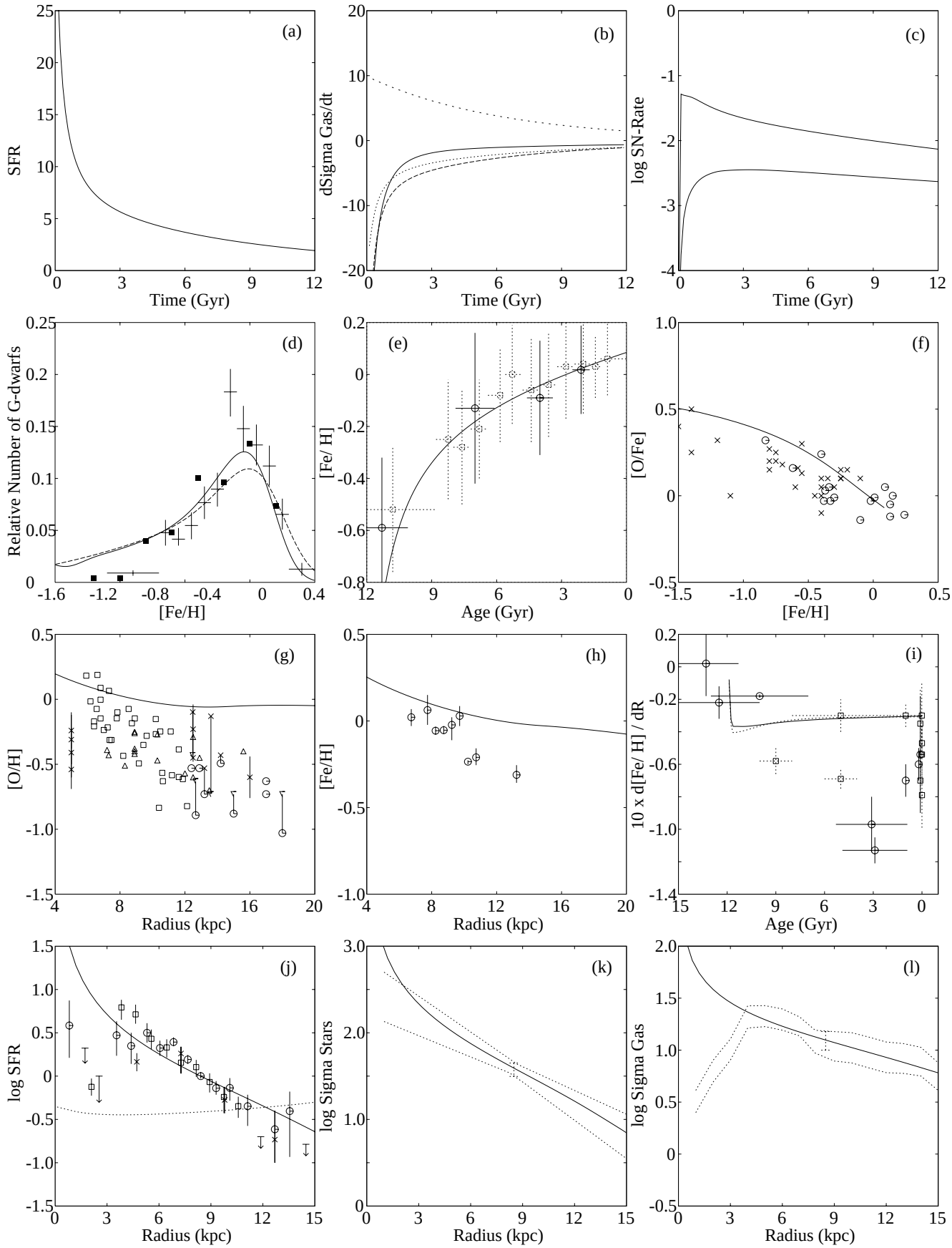

Fig. 5a–l. Properties of the model 1 from Table 4 with a standard initial disk profile and parameters $(a, b, \beta, i, t_i) = (1, 2, 0.5, 0.5, 6.4\,\mathrm{Gyr})$. A detailed description of panels **a** to **l** is given in Sect. 4.2.1.

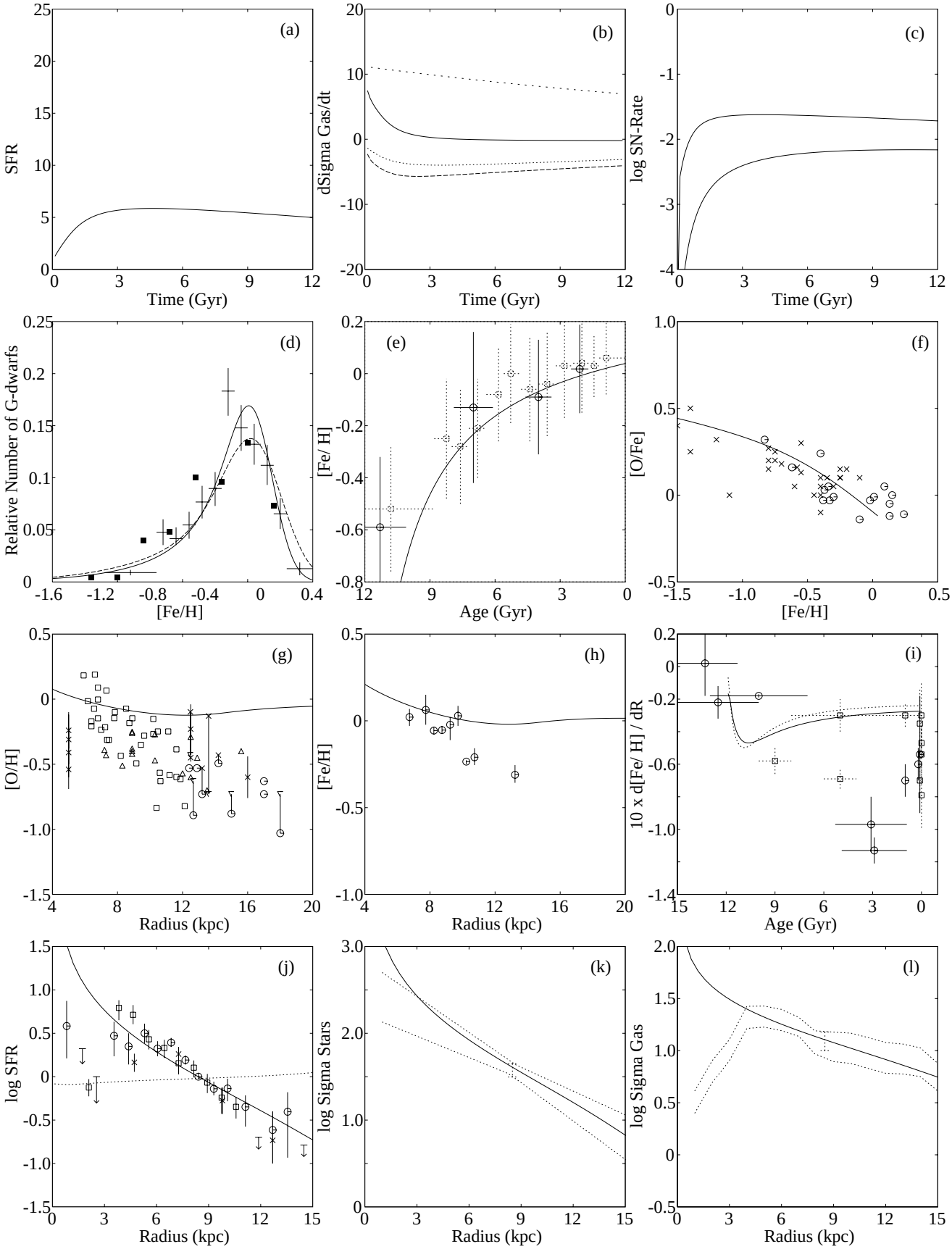

Fig. 6a–l. As in Fig. 5a–l, but for model 4 from Table 4 with parameters $(a, b, \beta, i, t_i) = (1, 2, 0.5, 0.95, 25.6\,\mathrm{Gyr})$.

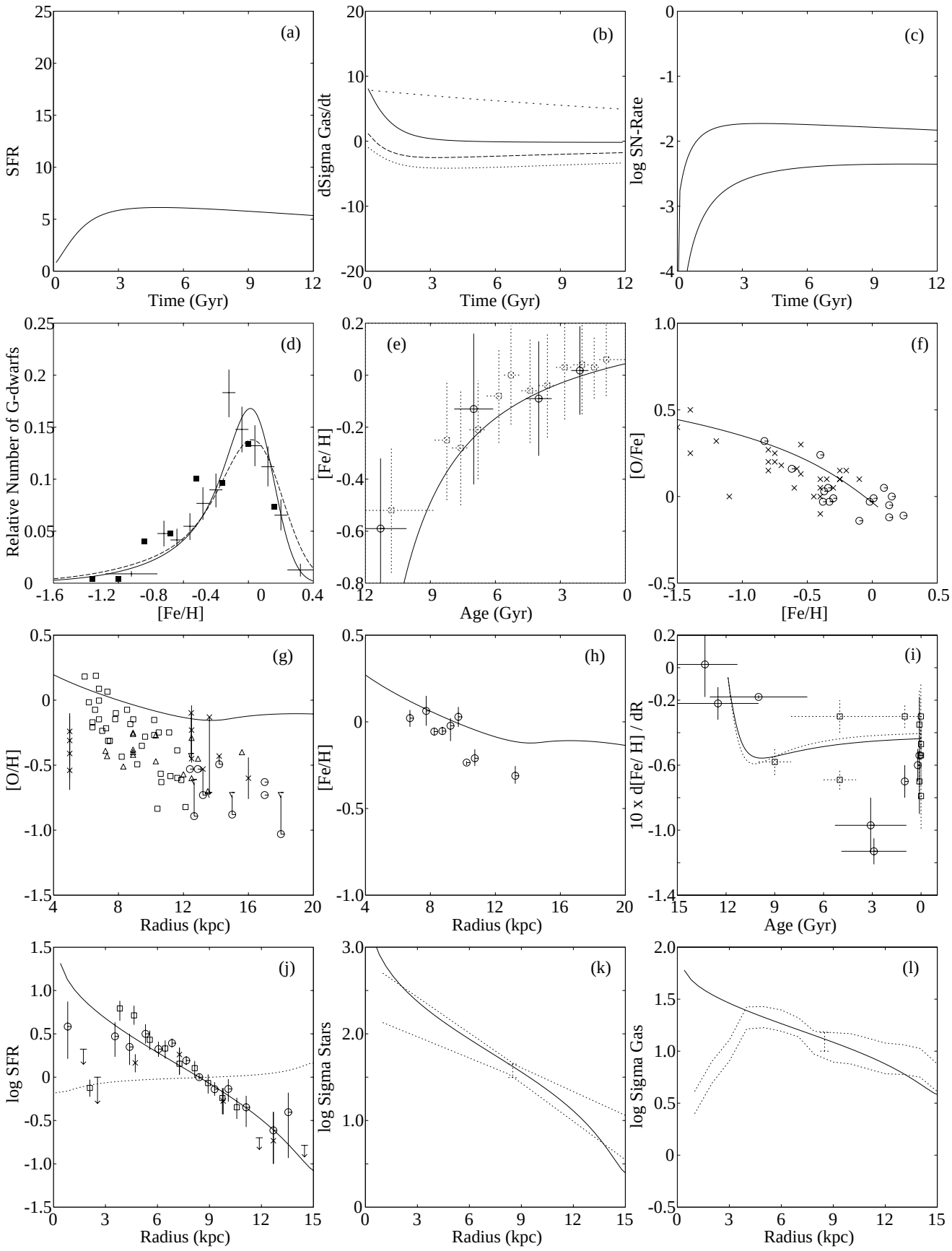

Fig. 7a–l. As in Fig. 5a–l, but for model 5 from Table 4 with parameters $(a, b, \beta, i, t_i) = (1, 2, 0.18, 0.95, 25.6\,\mathrm{Gyr})$ and with an infall-induced gas flow for $v_\phi^{inf}/v_\phi = 0.8$.

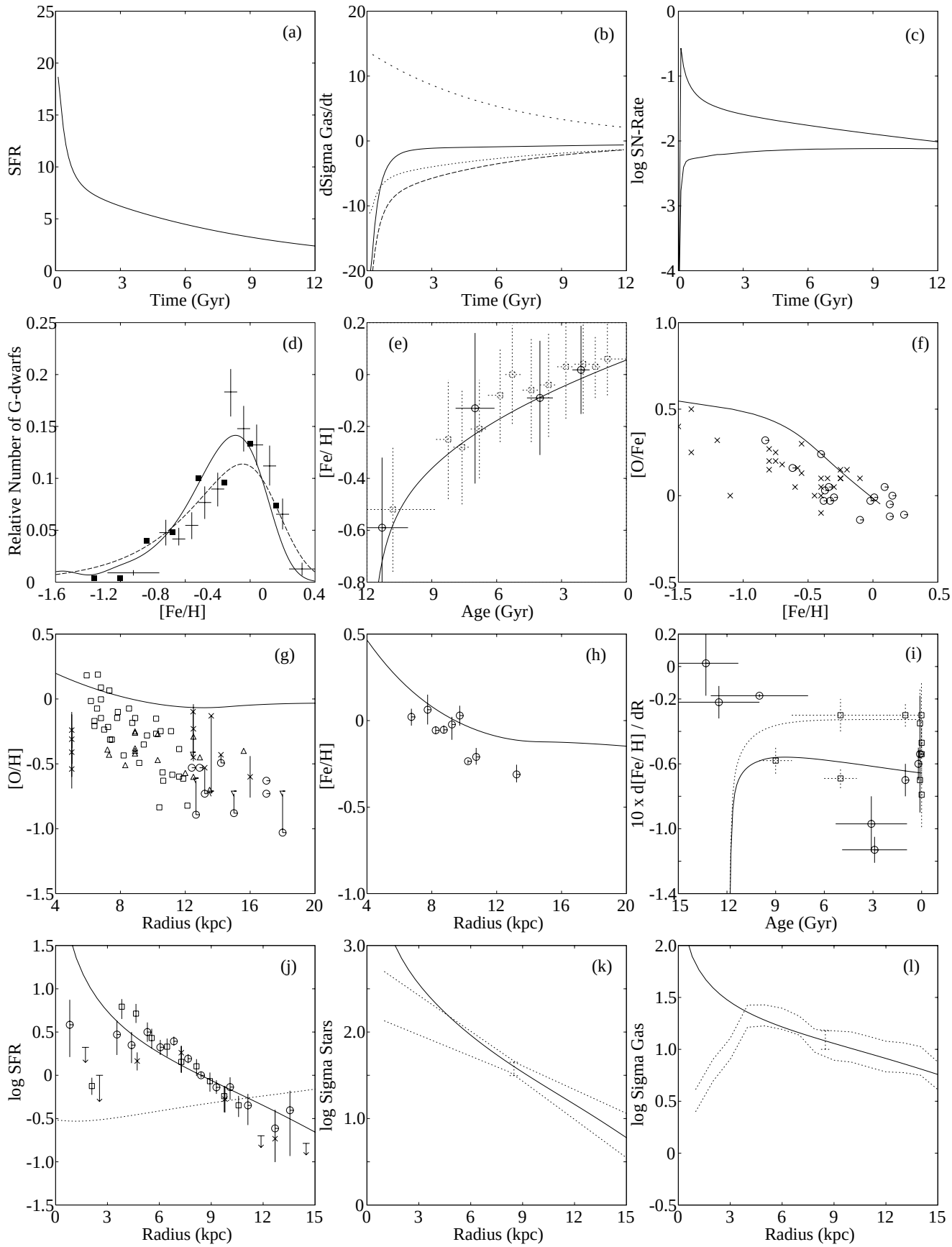

Fig. 8a–l. As in Fig. 5a–l, but for model 8 from Table 4 with parameters $(a, b, \beta, i, t_i) = (1, 2, 0.5, 0.5, 6.4\,\mathrm{Gyr})$ and an initial exponential disk density profile with a scalelength of 2 kpc.

Table 4. Parameters for 8 good-fit models.

model	(1)	(2)	(3)	(4)	(5)	(6)	(7)	(8)
(a, b, β)	(1,2,0.5)	(1,2,0.5)	(1,2,0.5)	(1,2,0.5)	(1,2,0.18)	(0,1,0.5)	(2,3,0.5)	(1,2,0.5)
$(i, t_i$/Gyr)	(0.5, 6.4)	(0.95,6.4)	(0.50, 25.6)	(0.95, 25.6)	(0.95,25.6)	(0.95,25.6)	(0.95, 25.6)	(0.5, 6.4)
v_ϕ^{inf}/v_ϕ	1	1	1	1	0.8	1	1	1
$\Sigma_0(R)$	standard	standard	standard	standard	standard	standard	standard	expo2
ν_0	$6.0\,10^{-3}$	$1.0\,10^{-2}$	$6.0\,10^{-3}$	$1.5\,10^{-2}$	$5.5\,10^{-3}$	1.5	$1.5\,10^{-4}$	8.0^{-3}
A	$1.6\,10^{-1}$	$2.2\,10^{-1}$	$1.6\,10^{-1}$	$3.0\,10^{-1}$	$2.5\,10^{-1}$	$3.0\,10^{-1}$	$3.5\,10^{-1}$	1.1^{-1}
$m_{tot,1}$	$6.3\,10^{10}$	$6.3\,10^{10}$	$6.3\,10^{10}$	$6.3\,10^{10}$	$5.0\,10^{10}$	$6.3\,10^{10}$	$6.8\,10^{10}$	8.8^{10}
$m_{d,1}(R > 15)$	$1.2\,10^{10}$	$1.2\,10^{10}$	$1.2\,10^{10}$	$1.0\,10^{10}$	$3.4\,10^{9}$	$0.9\,10^{10}$	$1.2\,10^{10}$	1.1^{10}
$m_{b,1}$	$1.0\,10^{10}$	$1.0\,10^{10}$	$1.0\,10^{10}$	$1.2\,10^{10}$	$4.3\,10^{9}$	$1.3\,10^{10}$	$1.3\,10^{10}$	2.5^{10}
$l_*(R_\odot, t_1)$	3.9	3.8	3.9	3.6	3.4	3.6	3.5	3.1
$l_g(R_\odot, t_1)$	8.5	8.7	8.5	7.5	7.2	7.2	7.6	8.4
$\Psi(R_\odot, t_1)$	1.9	3.0	2.6	4.45	5.4	4.6	4.7	2.4
$b(R_\odot, t_1)$	0.39	0.58	0.56	0.95	0.99	0.97	0.94	0.46
$I(R_\odot, t_1)$	1.5	2.9	3.3	6.2	4.9	6.2	6.8	2.1
$d[O/H]/dR(t_1)$	-0.031	-0.033	-0.025	-0.024	-0.041	-0.022	-0.025	-0.033
$d[Fe/H]/dR(t_1)$	-0.03	-0.037	-0.022	-0.028	-0.044	-0.025	-0.029	-0.066
SN II rate	0.007	0.011	0.010	0.015	0.017	0.018	0.018	0.010
SN Ia rate	0.002	0.004	0.003	0.008	0.008	0.006	0.007	0.008
$v_R(R_\odot, t_1)$	-0.66	-1.1	-0.66	-0.94	-0.94	-1.16	-1.25	-0.84

$\Sigma_0(R)$ means the initial density profile, where "expo2" denotes the exponential profile with a scalelength of 2 kpc. l_*, l_g are the resulting scalelengths of the stellar disk and the gaseous disk, respectively, in kpc; The SFR Ψ and the infall rate I are in $m_\odot$ pc^{-2} Gyr^{-1}; The abundance gradients are given for t_1 and $6 \le R \le 10$ kpc in dex kpc^{-1}; $m_{tot,1}$: final total mass in $m_\odot$; $m_{d,1}(R > 15)$: mass in the final disk located outside the truncation radius of the initial disk; $m_{b,1}$: final mass within the central 3 kpc in excess to the exponential disk; SN rates are given in SNe per yr; v_R: radial velocity of the viscous gas flow at $R_\odot$ in km s^{-1}.

lar. Good fit models with other combinations (a, b) differ mainly in the bottom panels, i.e. the radial density profiles (see below). The parameters and the most interesting quantitative model results are listed in Table 4. For all models from Table 4 we adopted a radial density profile for the infalling gas, $\Sigma_0^i(R)$, (Eq. 15) according to the standard initial density profile of an isothermal sphere.

The 12 panels in Figs. 5 to 8 show the following: **(a)** The SFR at $R_\odot$. **(b)** The total temporal variation of the gas density at $R_\odot$ (solid curve) and its various components: net star formation rate Ψ_{net} (dotted), radial flow (long dashes), and infall of external gas (short dashes). **(c)** The total rate of SNe II (upper curve) and SNe Ia (lower curve) in the Galactic disk (number per yr). **(d)** The $[Fe/H]$ distribution of long-lived stars convolved with a Gaussian with constant dispersion (solid) and age-dependent dispersion (dashed), respectively (see Sect. 3.3); error crosses: Rocha-Pinto & Maciel (1996), filled squares: Wyse & Gilmore (1995). **(e)** The AMR; solid error crosses: Edvardsson et al. (1993), dotted crosses: Meusinger et al. (1991), rescaled to a disk age of 12 Gyr. **(f)** $[O/Fe]\ versus\ [Fe/H]$; open circles: Edvardsson et al. (1993), crosses: Barbuy & Erdelyi-Mendes (1989). **(g)** Radial oxygen abundance profile; open squares: Shaver et al. (1983), triangels: Kaufer et al. (1994), crosses: Kilian-Montenbruck et al. 1994, vertical bars connecting circles with triangles: Vílchez & Esteban (1996). **(h)** Iron abundance profile; circles: Piatti et al. 1995. **(i)** The abundance gradient, within the range $R = 6$ to 10 kpc, in dependence on age. Solid error bars and model curves for $[Fe/H]$, dotted for $[O/H]$; empirical data from Tab. 3. **(j)** The radial profile of the present-day SFR (normalized to the SFR in the solar cylinder ring). The empirical data were taken from Lacey & Fall (1985). The dotted line is the relative SFR parameter $b_1(t_1)$. **(k)** and **(l)** The present-day radial density profiles for stars and gas, respectively. The ranges allowed by observations are indicated by dotted curves, taken from Prantzos & Aubert (1995).

Similar good models were found for $\beta = 1$, except for the higher central mass (Sect. 4.1). Generally, models with higher β must have higher values for ν_0 in order to reproduce the present-day gas fraction. Because of $\Psi \propto \nu_0/\beta$, the history of the SFR is nearly the same for models with different β. At the solar position, the net effect of the stronger radial flow is a corresponding reduction of the local gas density which has to be balanced out by stronger gas infall. In models with $\beta = 1$, the present-day gas infall rate is therefore generally higher than for $\beta = 0.5$.

A closer inspection reveals that there is no parameter set for which the model predictions are in a perfect agreement with all observational constraints. Especially, the empirical ADF and the RAGs are only moderately fit by the models. Below, we will discuss some model properties in more detail.

4.2.2. ADF in the solar neighbourhood

It is worth noting that the effect of gas infall is coupled to the strength of viscous radial gas transport. In viscous models, the effect of infall is, therefore, slightly different from that in models without viscosity.

In Figs. 5 to 8, results from models are shown providing the best possible fit to the ADF. At the metal-poor tail

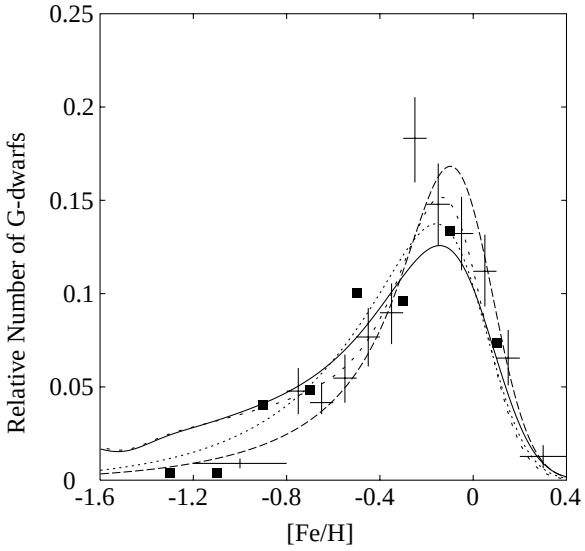

Fig. 9. The ADF from the four models 1 to 4 from Table 4 with $(a, b, \beta) = (1, 2, 0.5)$ but different gas infall parameters (i, t_i). Solid curve: $(0.5, 6.4\,\mathrm{Gyr})$, dotted: $(0.95, 6.4\,\mathrm{Gyr})$, short dashes: $(0.5, 25.6\,\mathrm{Gyr})$, long dashes: $(0.95, 25.6\,\mathrm{Gyr})$. To consider chemical inhomogeneities the model ADF has been convolved with a Gaussian with age-dependent dispersion (Sect. 3.3).

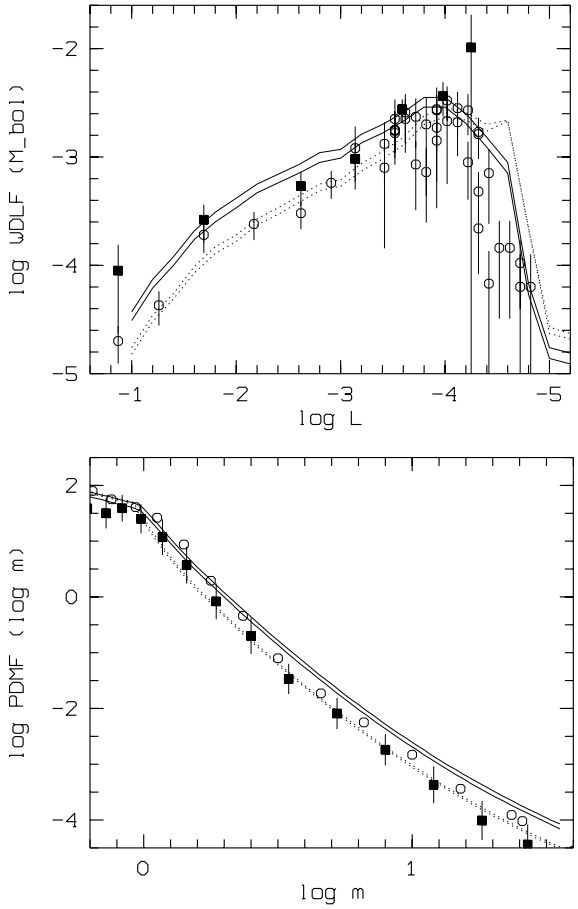

Fig. 10. WDLF (*top*) and PDMF (*bottom*) in the solar neighbourhood for the models shown in Figs. 5 to 8. Dotted curves: models with $(i, t_i) = (0.5, 6.4\,\mathrm{Gyr})$, corresponding to Figs. 5 and 8. Solid curves: models with $(i, t_i) = (0.95, 25.4\,\mathrm{Gyr})$, corresponding to Figs. 6 and 7. The empirical WDLF (filled rectangles: Evans 1992, open circles: Liebert et al. 1988) has been shifted by $+0.3$ dex in order to correct for the fact that white dwarfs in binaries may be under-represented in the observed WDLF (Yuan 1992). The empirical PDMF is taken from Scalo (1986) - filled rectangles with error bars and Basu & Rana (1992) - open circles. Luminosity L and mass m in solar units.

($[Fe/H] < -0.8$), the ADF is fit only by models with a long infall timescale, $t_i \approx 2t_1$, and a high infall fraction of $i = 0.95$ (cf. Fig. 9). The metal-rich part of the ADF is fit due to taking into account chemical inhomogeneities in the Galactic disk (cf. Sect. 3.3). The models are generally not able to reproduce the narrow peak of the Rocha-Pinto & Maciel (1996) ADF, neither its exact postition nor its small half-width. This is partly due to the rough parametrization of the SFR. Rocha-Pinto & Maciel proposed to explain the peak as due to a major star formation event about 8 Gyr ago. Star bursts do not naturally arise from the SFR described by Eq. (13). One should remember (Sect. 3.1), however, that the strong peak is not indicated by the data from Wyse & Gilmore (1995).

In models with a standard initial disk and a long infall timescale along with a high infall fraction, the relative SFR is near unity. However, the predicted present-day infall rate is $I(R_\odot, t_1) \approx 6\,\mathrm{m_\odot\,pc^{-2}\,Gyr^{-1}}$, i.e. uncomfortably high.

In models with a strongly concentrated initial disk profile, the ADF is approximated also for lower infall rates, i.e. i smaller, t_i shorter. The reason for that different behaviour is that the direction of the strong radial flows appearing in the early evolutionary stages at the solar distance depends on the initial density profile. For an exponential initial disk with a scalelength of 2 kpc (model 8, Fig. 8) we have a present-day infall rate of about $2\,\mathrm{m_\odot\,Gyr^{-1}\,pc^{-2}}$. Moreover, this model provides a better fit to the AMR at low metallicities, compared to the models with the standard initial disk and infall parameters $(i, t_i) = (0.95, 25.6\,\mathrm{Gyr})$.

4.2.3. PDMF and WDLF

The consistency of the IMF with the SFR can be checked considering simultaneously the PDMF of the nearby main-sequence stars and the WDLF (Yuan 1992; Meusinger 1994). The corresponding results for the models from Figs. 5 to 8 are shown in Fig. 10. In models with a high infall fraction and long infall timescales, the SFR in the solar cylinder ring starts on a low level, reaches a maximum after about 2 to 3 Gyr and remains nearly constant for the rest of the evolution (Figs. 5 to 8). As a consequence, the number of low-luminosity white dwarfs is reduced in such models as compared to models with a lower infall fraction and a shorter infall timescale. On the other hand, the present-day SFR is higher, resulting in larger numbers of white dwarfs with $\log L/L_\odot > -4$ as well as of massive main-sequence stars.

The strong decline toward low luminosities in the empirical WDLF from Liebert et al. (1988) has been interpreted by several authors (e.g., Wood 1992) as a strong hint to a disk age much less than 12 Gyr. However, taking into account the uncertainties of the observational data, as well as of the white dwarf cooling theory, on the one hand and the rigidity of the models, on the other hand, we find that our best-fit models are in an acceptable agreement with the observations (Fig. 10). Moreover, it is remarkable that the IMF, which was derived from chemical evolution constraints for $m \geq 1 m_{\odot}$ (Sect. 3.4), provides a PDMF in a quite good agreement with the empirical PDMF.

4.2.4. Radial density profiles

In general, the gas density profile becomes too flat in models with $b - a \leq 0$, and too steep in models with $b - a > 1$, respectively. The observed radial gas density profiles, as well as the SFR show a characteristic turnover at $R \approx 4$ kpc. This feature is not reproduced by the models with $b - a = 1$ without further assumptions. This point will be discussed below (Sect. 5.2) in more detail.

Radial profiles are, in general, only moderately affected by infall according to Eq. (15). For the standard initial disk with a truncation radius r_t between 10 and 20 kpc, the final disk always shows a ratio $l_*/r_t \approx 0.25$. This is in near agreement with the mean value of 0.20 found by Olivier et al. (1991) for viscous models without infall.

Different initial density profiles result in nearly the same final density profiles. This is illustrated by the comparison of Fig. 5 (standard disk) with Fig. 8 (exponential disk with scalelength 2 kpc).

4.2.5. RAGs

The row next to the bottom in Figs. 5 to 8 shows the radial profiles of $[O/H]$ and $[Fe/H]$, along with the time-dependence of the O- and Fe-abundance gradients.

It should be noticed that there seems to be a discrepancy between the abundances measured in nearby H II regions (e.g., Orion) and in nearby young stars. This problem has been addressed already by Shaver et al. (1983) and many others (Trimble 1991; Wilson & Matteucci 1992; Fitzsimmons et al. 1992; Ferrini et al. 1994; Prantzos & Aubert 1995). According to the AMR and the $[Fe/H]$–$[O/H]$ relation the oxygen abundance of the youngest stars is $[O/H] \approx 0$, i.e. solar. This value is clearly higher than the abundance expected for $R_{\odot}$ from the $[O/H]$ data of H II regions. Depletion on to dust grains may account for a part of this discrepancy (perhaps up to 0.3 dex, see Fitzsimmons et al. 1992), however, the situation is not quite clear. Therefore, we follow the approach by Prantzos & Aubert (1995) and restrict the evaluation of the abundance profiles to the gradients only instead of the absolute values for the abundances.

Viscous disk models are known to produce only weak abundance gradients (Sommer-Larsen & Yoshii 1990). For models with a lower infall fraction ($i = 0.5$) and a short infall timescale ($t_i = 6.4$ Gyr) we find oxygen gradients of about -0.03 to -0.04 dex kpc^{-1}, in agreement with the results from the models presented by Tsujimoto et al. (1995b). These gradients are definitely too small when compared with the "classic" observational result for the oxygen gradient from Shaver et al. (1983). Nevertheless, with regard to the broad scatter in the observed gradients (Table 3), we find that the model gradients are still within the limits of the observational uncertainties. However, for models with $(i, t_i) = (0.95, 25.4\,\mathrm{Gyr})$, which provide a better solution of the G dwarf problem, the RAGs are further reduced to the range $-0.02 ... -0.03$ dex kpc^{-1}.

There are several processes which may, in principle, provide a contribution to the RAGs: First, if the rotation velocity of the infalling gas is lower than the disk rotation velocity at the radial position of the infall, $v_{\phi}^{inf}(R) < v_{\phi}(R)$, an additional radial gas flow occurs toward the centre (Eq. 8). Fig. 7 shows a model with $v_{\phi}^{inf}/v_{\phi} = 0.8$. In this model, the viscosity ν_0 (and, therefore, the parameter β, see Sect. 4.2.1) has been reduced to avoid a much too strong mass concentration toward the centre. As can be seen by comparing Fig. 7(i) with Fig. 6(i), the RAGs are slightly larger in that case. Moreover, if the initial disk profile is steeper than the standard profile, steeper abundance profiles are formed. For instance, adopting in model 1 an exponential initial disk instead of the standard profile, the iron gradient is enhanced by -0.015 dex kpc^{-1} for a scalelength $l_0 = 4$ kpc and by -0.033 dex kpc^{-1} for $l_0 = 2$ kpc, respectively (cf. Fig. 8). The resulting oxygen gradient, on the other hand, is not significantly influenced by this initial condition. Finally, a further amplification of the abundance gradients is expected if star formation is a threshold process (e.g., Clarke 1989; Chamcham & Tayler 1994). This idea will be followed in a more self-consistent way in the context of another family of viscous models which will be the subject of a separate study.

In models with the standard initial disk, evolution starts with a shallow abundance profile. Due to quick gas redistribution, stronger gradients are formed quickly, and the RAGs are slightly reduced due to the viscous flow and viscous diffusion throughout the rest of the evolution (cf. Sect. 4.1). While the former feature seems to agree with observational evidence, the latter one does not (Sect. 3.3). In the case of an exponential initial disk profile with a short scalelength (model 8), the situation is a little bit different: At the very beginning, the abundance profiles are very steep, but are quickly reduced. The time interval of the strong RAGs is so short (a few 10^8 yr) that it seems impossible to observe strong RAGs for old disk objects. The iron RAG becomes slightly enhanced throughout further evolution while the oxygen RAG is rather constant.

5. The inner part of the Galaxy

5.1. The bulge - a continuation of the inner viscous disk?

The overexponential increase of stellar mass in the inner few kpc predicted by viscous evolution models has been related to the Galactic bulge (Yoshii & Rodgers 1989; Weinberg 1992; Tsujimoto et al. 1995a; Courteau et al. 1996). In order to test the hypothesis of the origin of the Galactic bulge from viscous flows

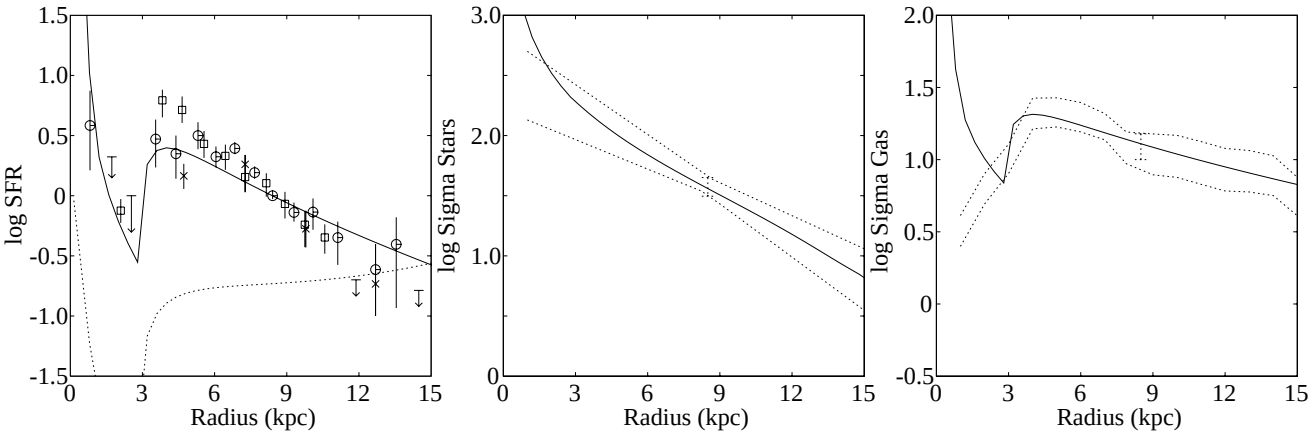

Fig. 11. Model 1 from Table 4 has been modified to simulate the effect of a temporary central bar potential by strongly enhancing the viscosity in the inner 2.5 kpc during the last 3 Gyr. *Left:* SFR (solid curve) and relative SFR (dotted curve), *middle:* stellar density, *right:* gas density.

in the disk, we examine the age and metallicity properties of the central mass concentration in the models (i.e. in the "model bulge").

For the four models shown in Fig. 9 the age distribution of the stars in the inner few kpc shows a maximum at $10...11$ Gyr, a broad wing toward younger ages, and a mean age of about 6 to 7 Gyr. HST observations have shown that bulge and halo globular clusters appear coeval (Ortolani et al. 1996). A high bulge age of 14 ± 1 Gyr has also been derived from spectra of the integrated light in Baade's window (Idiart et al. 1996). On the other hand, the observations of a component of young stars (e.g., Paczynski et al. 1994; Glass et al. 1995) agrees with our model predictions.

As a consequence of a higher initial SFR, the metal enrichment proceeds on a short timescale in the inner few kpc. The AMR reaches solar metallicity already after about 3 Gyr and rises up further thereafter. The SFR remains on a high level because the radial gas drift continuously delivers gas into the central region. For instance, the mean value of the $[Fe/H]$-distribution of the long-lived stars is between 0.3 and 0.4 dex for the four models from Fig. 9. This value is approximately equal to the average abundance of bulge K giants found by Rich (1988). However, the recalibration of the abundance scale based on high resolution spectra and updated model atmospheres (McWilliam & Rich 1994) yields a significantly different distribution with a mean $[Fe/H] \approx -0.2$ and a broad dispersion of $\sigma_{[Fe/H]} = 0.4$ (cf. also Ibata & Gilmore 1995; Minniti et al. 1995; McWilliam 1997).

The available abundance statistics still suffer from uncertainties, especially due to the small number statistics. More data for the alpha element abundances are desirable. However, with respect to the abundance distribution found by McWilliam & Rich (1994), the chemical properties of the "model bulge" are clearly inconsistent with its identification with the Galactic bulge. The age distribution seems also to disagree with what is indicated by observations. The high central gas fraction in the models apparently provides a further objection against such an interpretation. However, the inner gas density profile may be significantly changed if a central bar is taken into account (see below).

Nevertheless, there are two possibilities to relate the surplus of the model stellar mass concentration with the Galactic bulge: *Firstly*, only a fraction of the Galactic bulge, in particular the younger, more metal-rich stars, originate from the steady star formation in the gas supplied by the viscous gas flow. Then, we have to assume that galactic bulges were formed due to distinct processes (cf. Wyse et al. 1997). In particular, additional gas transport toward the central region can be triggered by interactions with a satellite (Martin 1995) which will also heat up disk stars and induce the formation of a bulge-like component (Courteau et al. 1996, and references therein). The interpretation of the central mass surplus as a fraction of the bulge should be related to models with $\beta = 0.5$. In these models, the stellar surplus mass is reduced by a factor of two to three with respect to models with $\beta = 1$ to a mass of about $10^{10}\,\mathrm{m}_\odot$ (Table 4). This corresponds to about 1/4 to 1/2 of the mass of the Galactic bulge (Blum 1995). As was shown above, models with $\beta = 0.5$ reproduce most of the observed properties of the Galactic disk.

Secondly, the central stellar mass surplus can be identified with the whole Galactic bulge only under the assumption that it has been created in about the first Gyr. Indeed, the viscous flows toward the center are very strong during the first Gyr. Subsequent gas supply due to infall and viscous flow may provide the material for the formation of the innermost part of the disk and for a smaller fraction of younger bulge stars. For $\beta = 1$, models with a standard initial disk produce a "bulge" with a mass of a considerable fraction of the disk mass (but also a strong flow through the inner boundary). With respect to the present-day gas infall rates, this second possibility seems less acceptable, especially if the standard initial disk is adopted: As mentioned above (Sect. 4.2.1), models with stronger radial gas flows require stronger gas infall. Thus, the present-day infall rate for good fit models with $\beta = 1$ is about a factor of two higher than that for $\beta = 0.5$. As noted in Sect. 4.2.2, the infall rate for the latter models is, however, already quite high compared to the limits set by observations. This problem is considerably

reduced adopting an exponential initial disk profile with a short scalelength as in model 8 from Table 4. (In this case, the initial mass is about half the final disk mass.)

5.2. The central bar

Optical surveys as well as infrared observations reveal that the majority of disk galaxies have a bar (Zaritsky et al. 1993; Martin 1995). Barred spirals show significantly shallower radial abundance profiles than spirals without a bar (e.g., Vila-Costas & Edmunds 1992; Oey & Kennicut 1993; Zaritsky et al. 1994). The strength of the gradients seems to be directly correlated to the strength of the bars (Martin & Roy 1994). This may be interpreted as chemical homogenisation of the ISM due to radial gas flows (Pagel et al. 1979).

The dynamics of the gas influenced by a bar is very complicated. The simple parametrization of the viscosity is obviously not suitable to reproduce the gas density distribution in the inner region of the Galactic disk, especially in the presence of a bar. For this reason we restrict our discussion to a level of qualitative simulations.

The enhanced cloud-cloud collision rate due to a bar potential leads to fast gas transport towards the centre and creates a gas-depleted zone. This effect is formally described as enhanced viscosity. If the viscosity is significantly increased for $R < 3\,\mathrm{kpc}$, our models predict radial profiles of gas density and SFR which approximately fit the observed profiles with their local maxima at $R \approx 4\,\mathrm{kpc}$ (Fig. 11). The stellar component is expected to show a similar radial density distribution if the bar is present all the time. However, the stellar density profile in the inner disk is established essentially in the early evolutionary phase. Thus, we find that the model stellar disk is very similar to that in the standard model (i.e. exponential + central mass concentration) if the bar is a transient phenomenon in later evolutionary stages. As expected, the RAGs are significantly reduced due to the bar in the inner few kpc, but are essentially unchanged for $R \geq 5\,\mathrm{kpc}$.

6. Conclusions

We have studied models for the long-term evolution of the Galactic disk which include viscous radial gas flows, gas infall, and infall-induced gas flows. The model predictions were confronted with a large set of observational constraints. Hybrid infall/viscous flow models were found to reproduce most of the relevant observations, at least roughly. Especially, the models can explain

- the "conspiracy" between the dark halo-dominated outer rotation curve and the disk/bulge-dominated inner rotation curve,
- exponential radial stellar density profiles independent of the initial disk profile,
- radial profiles of gas and SFR, respectively, which are in agreement with observational constraints over a wide R range,
- the existence of RAGs.
- local constraints, including the ADF, AMR, PDMF, WDLF, and $[O/H]$–$[Fe/H]$ relation, are at least approximated by the models. Owing to the simple description of the SFR, not all details of the observational constraints are well-fit by the models. This holds especially for the narrow peak in the G dwarf abundance distribution found by Rocha-Pinto & Maciel (1996). We find a generally better agreement with the observations in models starting from a steep exponential initial gas density profile instead of the standard assumption of the density profile of an isothermal sphere.

With typically $-0.003\,\mathrm{dex\,kpc^{-1}}$, the RAGs predicted by viscous models are small compared to observational results. On the other hand, the available observational data on RAGs in the Galactic disk are still beset with large uncertainties. The model gradients may be enhanced when infall-induced radial gas flows are involved. Moreover, the iron RAG is significantly larger if an exponential initial gas distribution with a short scalelength is adopted instead of an isothermal sphere. The model RAGs are nearly constant with time which contradicts the indications for shallower abundance profiles for older disk stars. Besides the values for the RAGs, the time-evolution of the abundance profiles may provide a crucial test for viscous evolution models.

The viscous radial gas drift generates a central stellar mass concentration in excess of the exponential stellar disk profile. In models with $\beta \approx 0.5$ and the standard initial disk, the central mass concentration is consistent with its interpretation as a fraction of the Galactic bulge. The alternative model with a steep exponential initial disk generates a central mass component which may be identified with the whole bulge on the condition that is was formed in a very early evolutionary stage. It is tempting to speculate that it is essentially a large fraction of this initial disk what evolves into the bulge.

Viscous models predict high gas densities in the inner few kpc contrary to what is observed for the disk of our Galaxy. However, this discrepancy may be considerably reduced if the viscosity is temporary strongly enhanced in the inner region, e.g. due to a transient central bar.

We have not yet considered the effects of a star formation threshold and the existence of an outer cut-off in the stellar density profile. These items will be the subjects of a subsequent study on an alternative family of viscous models, which take into account self-regulation of the star formation process.

Acknowledgements. We thank H.-E. Fröhlich, G. Hensler, J. Köppen, P. Kroupa, E. Müller, and Ch. Theis for valuable discussions. S. Klose has examined the basic equations in an earlier version of the models. The anonymous referee is thanked for several valuable comments which have helped to significantly improve the paper. This research was supported by the Deutsche Forschungsgemeinschaft.

Appendix A: derivation of Eq. (8)

In this Appendix, we derive the expression for the velocity v_R of the radial viscous drag in the gaseous component of a star forming galactic disk undergoing gas infall (Eq. 8).

For a closed system of force-free particles of a compressible gas the momentum balance is given by (e.g. Landau & Lifshitz 1963)

$$\frac{\partial}{\partial t}(v_i\Sigma) + \frac{\partial}{\partial x_j}(v_i\Sigma)v_j = \frac{\partial}{\partial x_j}\sigma_{ij}, \quad \text{(A1)}$$

with the stress tensor

$$\sigma_{ij} = -p\delta_{ij} + \eta\Big[\frac{\partial v_i}{\partial x_j} - \frac{2}{3}\delta_{ij}\frac{\partial v_l}{\partial x_l}\Big] + \zeta\delta_{ij}\frac{\partial v_l}{\partial x_l}, \quad \text{(A2)}$$

η and ζ are the coefficients of the viscosity. The sum convention is used. Σ is the gas density; for the sake of clearness we do not use the index g.

For a realistic Galactic disk model we have to take into account the effects of gas infall and interaction between the gaseous and the stellar component. Assuming that the velocity of the infalling gas is constant with time, its contribution to the momentum balance is $\frac{\partial}{\partial t}(\boldsymbol{v}^{inf}\Sigma^{inf}) = \boldsymbol{v}^{inf}I$. Condensation of gas into stars with the rate Ψ_{net} removes from the gas the momentum $\Psi_{net}\boldsymbol{v}$. On the other hand, momentum input due to SNe and stellar winds is not described by a separate production term because it is already considered by the viscous stress tensor. (Note that the interpretation of the viscosity is based on the interaction between the stellar and and the gaseous component.) Therewith, we have the momentum balance

$$\frac{\partial}{\partial t}(v_i\Sigma) + \frac{\partial}{\partial x_j}(v_i\Sigma)v_j = \frac{\partial}{\partial x_j}\sigma_{ij} + v_i^{inf}I - v_i\Psi_{net}, \quad \text{(A3)}$$

the balance for the gas mass

$$\frac{\partial}{\partial t}\Sigma + \frac{\partial}{\partial x_j}(v_j\Sigma) = I - \Psi_{net}, \quad \text{(A4)}$$

and, from the combination of both, the transport equation

$$\Sigma\Big[\frac{\partial v_i}{\partial t} + v_j\frac{\partial v_i}{\partial x_j}\Big] = [v_i^{inf} - v_i]I + \frac{\partial}{\partial x_j}\sigma_{ij} \quad \text{(A5)}$$

Now, let us consider the Φ-components of Eqs. (A3) and (A5):

$$\frac{\partial}{\partial t}(v_\Phi\Sigma) + \frac{1}{R}\frac{\partial}{\partial R}(R\Sigma v_R v_\Phi) + \frac{1}{R}\Sigma v_R v_\Phi = [v_\Phi^{inf} - v_\Phi]I - \Psi_{net}v_\Phi + \frac{1}{R^2}\frac{\partial}{\partial R}\Big(R^3\nu\Sigma\frac{\partial}{\partial R}\frac{v_\Phi}{R}\Big), \quad \text{(A6)}$$

$$\Sigma\frac{\partial v_\Phi}{\partial t} + \Sigma v_R\Big[\frac{\partial v_\Phi}{\partial R} + \frac{v_\Phi}{R}\Big] = [v_\Phi^{inf} - v_\Phi]I + \frac{1}{R^2}\frac{\partial}{\partial R}\Big(R^2\Sigma\nu\Big[\frac{\partial v_\Phi}{\partial R} - \frac{v_\Phi}{R}\Big]\Big), \quad \text{(A7)}$$

where we replaced the dynamic viscosity η by the kinematic viscosity $\nu = \eta/\Sigma$. The last equation transforms easily into Eq. (8).

Now we show that Eqs. (A6) and (A7) give the relations used in other studies for the special cases of either vanishing infall or vanishing viscosity. If we consider a closed gaseous disk without star formation and use $\Omega = v_\Phi/R$, Eq. (A6) reads

$$\frac{\partial}{\partial t}\Big(\Sigma R\Omega\Big) + \frac{1}{R^2}\frac{\partial}{\partial R}\Big(R^3\Sigma v_R\Omega\Big) = \frac{1}{R^2}\frac{\partial}{\partial R}\Big(R^3\nu\Sigma\frac{\partial\Omega}{\partial R}\Big). \quad \text{(A8)}$$

After multiplication by R, Eq. (A8) gives the Eq. (2.8) in Pringle (1981). Sommer-Larsen & Yoshii (1989) describe the viscous evolution of a closed system with constant rotation curve. In this case our Eq. (A7) is reduced to

$$\Sigma v_R\Big[R\frac{\partial\Omega}{\partial R} + 2\Omega\Big] = \frac{1}{R^2}\frac{\partial}{\partial R}\Big(\eta R^3\frac{\partial\Omega}{\partial R}\Big). \quad \text{(A9)}$$

Adopting Sommer-Larsen & Yoshii's parametrization of the rotation curve $\Omega = \Omega_0 R^{-\alpha}$ we have

$$v_R = -\frac{\alpha}{2-\alpha}\nu\Big[\frac{1}{\Sigma}\frac{\partial\Sigma}{\partial R} + \frac{1}{\nu}\frac{\partial\nu}{\partial R} + \frac{2-\alpha}{R}\Big], \quad \text{(A10)}$$

which is easily transformed into Eq. (12) in Sommer-Larsen & Yoshii (1989).

Finally, we consider the case of a disk with vanishing viscosity but undergoing infall. The rotation curve should be constant in time. This corresponds to the models investigated by Pitts & Tayler (1989) and Chamcham & Tayler (1994). From Eq. (A7) we find

$$\Sigma v_R\Big[\frac{\partial v_\Phi}{\partial R} + \frac{v_\Phi}{R}\Big] = I[v_\Phi^{inf} - v_\Phi]. \quad \text{(A11)}$$

Replacing v_Φ by the specific momentum $h = Rv_\Phi$ we have

$$\Sigma v_R\frac{\partial h}{\partial R} = I[h^{inf} - h], \quad \text{(A12)}$$

in agreement with Eq. (4) in Chamcham & Tayler (1994).

References

Alfaro E. J., Cabrera-Cañ o J., Delgado A.J. 1993, ApJ 402, L53
Afflerbach A., Churchwell E., Acord J.M. et al. 1996, ApJS 106, 423
Afflerbach A., Churchwell E., Werner M. W. 1997, ApJ 478, 190
Bahcall J.N., Schmidt M., Soneira R.M. 1982, ApJ 258, L 23
Barbuy B., Erdelyi-Mendes M. 1989, A&A 214, 239
Basu S., Rana N.C.: 1992, Astrophys. J. 393, 373
Blum R.D. 1995, ApJ 444, L89
Boulares A.:1989, A&A 209, 21
Briggs F.H.: 1990, AJ 100, 999
Burton W. B. 1992, In: The Galactic Interstellar Medium, W. B. Burton, B. G. Elmegreen, R. Genzel (eds.), Berlin etc., Springer, p.1
Cappellaro E., Turatto M., Benetti S., et al. 1993, A&A 268, 472
Carlberg R.G., Dawson P.C., Hsu T., VandenBerg D.A. 1985, ApJ 294, 674
Carraro G., Chiosi C. 1994, A&A 287, 761
Chamcham K., Tayler R.J. 1994, MNRAS 266, 282
Clarke C. 1989, MNRAS 238, 283
Courthau S., De Jong R.S., Broeils A.H. 1996, ApJ 457, L73
Dame T.M. 1993, In: Back to the Galaxy, S. Holt, F. Verter (eds.), AIP, p. 267
De Marchi G., Paresce F. 1997, ESO preprint 1206
Duquennoy A., Mayor M. 1991, A&A 248, 485
Edmunds M.G. 1975, ApSS 32, 483
Edvardsson B., Andersen J., Gustafsson B. et al. 1993, A&A 275, 101

Evans D.W. 1992, MNRAS 255, 521
Firmani C., Hernandez X., Gallagher J. 1996, A&A 308, 403
Fröhlich H.-E. 1994, A&A 289, 749
Fitzsimmons A., Dufton P.L., Rolleston W.R.J. 1992, MNRAS 259, 489
Gilmore G., Wyse R., Kuijken K. 1990, In: Population, Age and Dynamics of the Galaxy, p. 172
Glass I.S., Whitelock P.A., Catchpole R.M., Feast M.W., 1995, MNRAS 273, 383
Greggio L., Renzini A. 1983, A&A 118, 217
Grevesse N., Anders E. 1989, AIP Conf. Ser. 183, American Institute of Physics, p. 1
Gunn J.E. 1982, In: Cosmology and Fundamental Physics, M.S. Longair, G.V. Coyne, H.A. Bruck (eds.), Citta del Vaticano, 233
Hensler G., Samland M., Theis C., Burkert A. 1994, In: Panchromativ view of galaxies, G. Hensler, C. Theis, J. Gallagher (eds.), Editions Frontières, 341
Ibata R.A., Gilmore G.F. 1995, MNRAS 275, 605
Idiart T.P., De Freitas Pacheco J. A., Costa R. D. D. 1996, AJ 111, 1169
Isern J., Hernanz M., Garcia-Berro E., et al. 1997, In: The History of the Milky Way and its Satellite System, A. Burkert, D. Hartmann, S.R. Majewski (eds.), ASP Conf. Ser. 112, p. 181
Janes K.A., Tilley C., Lynga G. 1988, AJ 95, 771
Janes K.A., Phelps R.L. 1994, AJ 108, 1773
Jimenez R., Thejll P., Jørgensen U. G., MacDonald J., Pagel B. 1996, MNRAS 282, 926
Kaufer A., Szeifert Th., Krenzin R., et al. 1994, A&A 289, 740
Kennicutt R.C. 1989, ApJ 344, 658
Kennicutt R.C., Garnett D.R. 1996, ApJ 456, 504
Kilian-Montenbruck J., Gehren T., Nissen P.E. 1994, A&A 291, 757
Köppen J. 1994, A&A 281, 26
Koester D., Reimers D. 1996, A&A 313, 810
Kroupa P. 1997, In: Brown Dwarfs and Extrasolar Planets, R. Rebolo, M.R. Zapatero Oserio, E. Martin (eds.), in press
Kroupa P., Tout C. A., Gilmore G. 1993, MNRAS 262, 545
Lacey C.G., Fall S.M. 1985, ApJ 290, 154
Landau L.D., Lifshitz E.M. 1963, Fluid Mechanics, Pergamon Press, Oxford
Larson R.B. 1972, Nature Phys. Sci. 236, 7
Lewis J.R., Freeman K.C. 1989, AJ 97, 139
Liebert J., Dahn C.C., Monet D.G.: 1988, ApJ 332, 891
Lin D.N.C., Pringle J.E. 1987, ApJ 320, L87
Lynden-Bell D. 1975, Vistas in Astronomy 19, 299
Maciel W. J., Köppen J. 1994, A&A 282, 436
Maeder A. 1992, A&A 264, 105
Majewski S.R. 1993, ARAA 31, 575
Majewski S.R., Phelps R.L., Rich R.M. 1997, In: The History of the Milky Way and its Satellite System, A. Burkert, D. Hartmann, S.R. Majewski (eds.), ASP Conf. Ser. 112, p. 181
Malinie G., Hartmann D.H., Clayton D.D., Mathews G.J. 1993, ApJ 413, 633
Martin P. 1995, AJ 109, 2428
Martin P., Roy J.-P. 1994, ApJ 424, 599
Martin P., Belley J. 1996, ApJ 468, 598
Matteucci F., Greggio L. 1986, A&A 154, 279
Matteucci F., Francois P. 1989, MNRAS 239, 885
Mayor M. 1976, A&A 48, 301
Mayor M., Vigroux L. 1981, A&A 98, 1
McWilliam A., Rich R. M. 1994, ApJS 91, 749
McWilliam A. 1997, ARA&A 35, 503
Meusinger H. 1994, Astron. Nachr. 315, 279
Meusinger H., Reimann H.-G., Stecklum B. 1991, A&A 245, 57
Meusinger H., Stecklum B. 1992, A&A 256, 415
Meusinger H., Schilbach E., Souchay J. 1996, A&A 312, 844
Minniti D., Olszewski E.W., Liebert J., et al. 1995, MNRAS 277, 1293
Muller R.A., Newberg H.J.M., Pennypacker C.R., et al. 1992, ApJ 382, L 9
Nissen P.E. 1995, In: Stellar Populations, P. C. van der Kruit, G. Gilmore (eds.), IAU, p. 109
Oey M.S., Kennicutt R.C. 1993, ApJ 411, 137
Olivier S.O., Blumenthal G.R., Primack J.R. 1991, MNRAS 252, 102
Ortolani S., Renzini A., Gilmozzi R., et al. 1996, In: Formation of the Galactic Halo...Inside and Out, H. Morrison, A. Sarajedini (eds.), ASP Conf. Ser. 92, p. 96
Paczynski B., Stanek K.Z., Udalski A., et al. 1994, AJ 107, 2060
Pagel B.E.J. 1989, In: Evolutionary Phenomena in Galaxies, J. Beckman, B.E.J. Pagel (eds.), Cambridge University Press, Ca,bridge, p. 201
Pagel B.E.J., Patchett B.E. 1975, MNRAS 172, 13
Pagel B.E.J., Edmunds M.G., Blackwell D.E., et al. 1979, MNRAS 189, 95
Pasquali A., Perinotto M. 1993, A&A 280,581
Pfenniger D., Combes F., Martinet L. 1994, A&A 285, 79
Piatti A., Clariá J.J., Abadi M.G. 1995, AJ 110, 2813
Pilyugin L.S., Edmunds M.G. 1996, A&A 313, 783
Pitts E., Tayler R.J. 1989, MNRAS 240, 373
Prantzos N., Aubert O. 1995, A&A 302, 69
Pringle J.E. 1981, ARAA 19, 135
Rana N. 1991, ARA&A 29, 129
Rich R. M. 1988 AJ 95, 828
Rocha-Pinto H.J., Maciel W.J. 1996, MNRAS 279, 447
Rocha-Pinto H.J., Maciel W.J. 1997, A&A 325, 523
Saio H., Yoshii Y. 1990, ApJ 363, 40
Salpeter E.E. 1955, ApJ 121, 161
Samland M., Hensler G., Theis, Ch. 1997, ApJ 476, 644
Scalo J.M. 1986, Fund. Cosmic Phys. 11,1
Schaller G., Schaerer D., Meynet G., Maeder A. 1992, A&A 266, 643
Schmidt M. 1963, ApJ 137, 758
Schuster W.J., Nissen P.E. 1989, A&A 222, 69
Shaver P.A., McGee R.X., Newton L.M., et al. 1983, MNRAS 204, 53
Simakov S.G. 1990, Pis'ma AZh 16, 679
Smartt S.J., Rolleston W.R.J. 1997, ApJ 481, L47
Smartt S.J., Dufton P.L., Lennon D.J. 1997, A&A 326, 763
Sommer-Larsen J. 1991, MNRAS 250, 356
Sommer-Larsen J. & Yoshii Y. 1989, MNRAS 238, 133
Sommer-Larsen J. & Yoshii Y. 1990, MNRAS 243, 468
Struck-Marcell C. 1991, ApJ 368, 348
Tammann G., Löffler W., Schröder A. 1994, ApJS 92, 487
Thorgensen E.N., Friel E.D. & Fallon B.V. 1993, PASP 105, 1253
Trimble V. 1991, A&A Rev. 3, 1
Tsujimoto T., Yoshii Y., Nomoto K., Shigeyama T. 1995 a, A&A 302, 704
Tsujimoto T., Nomoto K., Yoshii Y., et al. 1995 b, MNRAS 277, 945
Tsujimoto T., Yoshii Y., Nomoto K., et al. 1997, ApJ 483, 228
Twarog B.A., 1980, ApJ 242, 242
VandenBerg D.A. 1985, ApJS 58,711
van den Bergh S. 1962, AJ 67, 486
van den Hoek L.B., de Jong T. 1997, A&A 318, 231
van der Kruit P. 1989, In: The Milky Way as a Galaxy, R. Buser, I. King (eds.), Geneva Observatory, p. 334
Vila-Costas M.B., Edmunds M.G. 1992, MNRAS 259, 121
Vílchez J.M., Esteban C. 1996 MNRAS 280, 720

Wakker B.P., van Woerden H.: 1991, A&A 250, 509
Weidemann V. 1987, A&A 188, 74
Wielen R. 1977, A&A 60, 263
Wielen R., Fuchs B., Dettbarn C. 1996, A&A 314, 438
Wood M.A. 1992, ApJ 386, 539
Woosley S.E., Weaver T.A.: 1995, ApJS 101, 181
Wyse R.F.G., Silk J. 1989, ApJ 344, 658
Wyse R.F.G., Gilmore G. 1992, AJ 104, 144
Wyse R.F.G., Gilmore G. 1995, AJ 110, 2771
Wyse R.F.G., Gilmore G., Franx M. 1997, ARA&A 35, 637
Yoshii Y., Sommer-Larsen J. 1989, MNRAS 236, 779
Yuan J.W. 1992, A&A 261, 105
Zaritzky D., Rix H.-W., Rieke M. 1993, Nature 364, 313
Zaritsky D., Kennicutt R.C., Huchra J. P. 1994, ApJ 420, 87